ANALYTICAL AND NUMERICAL INVESTIGATION OF SPONTANEOUS IMBIBITION: A SENSITIVITY ANALYSIS ON THE EFFECT OF ROCK PROPERTIES AND BOUNDARY CONDITIONS

A Thesis

by

ABDUL SALAM ABD

Submitted to the Office of Graduate and Professional Studies of
Texas A&M University
in partial fulfillment of the requirements for the degree of

MASTER OF SCIENCE

Chair of Committee,	Ahmed Abdel-Wahab
Co-Chair of Committee,	Nayef Alyafei
Committee Members,	Albertus Retnanto
	Mohammed Nounou
Head of Department,	M. Nazmul Karim

May 2018

Major Subject: Chemical Engineering

ABSTRACT

In this research we present a numerical substitute for laboratory experiments through simulating a core sample fully bounded by the wetting phase to represent co-current and countercurrent spontaneous imbibition (SI) processes. We combine the results of the simulations with the analytical model for co-current and counter-current spontaneous imbibition developed by Karen Schmid in her 2011 study. to validate the upscaling of laboratory experiments to field dimensions using dimensionless time. We then present a detailed parametric study on the effect of boundary conditions and characteristic length to compare imbibition assisted oil recovery with different types of boundary conditions. We demonstrate that oil recovery was the fastest and highest when all faces are open to flow. We also demonstrate that all cases scale with the non-dimensionless time presented by Karen Schmid and Sebastian Geiger, and show a close match to the numerical simulation and the analytical solution.

Furthermore, the effects of the variations in the rock and fluid properties on the scaling group is studied in detail. We notice that the variations in different parameters including initial water saturation, oil/water viscosity ratios, oil/water relative permeability and wettability of the studied core did not affect the quality of the scaling of Karen Schmid and Sebastian Geiger's group, and the results matched accurately with the analytical solutions suggested., Moreover, we discuss how the effect of constructing a model with varying grid sizes and dimensions affects the accuracy of the results. We compare the results of the 2-D and 3-D models to observe that 3-D model proved superior in the

accuracy of the results on the expense of the CPU time to simulate a simple counter-current SI. Thus, we deduce that 2-D models yield satisfying results in a timely manner compared to 3-D models which are time-consuming.

Our work concluded that the new definition of non-dimensionless time work well with co-current and counter-current SI cases regardless of the boundary condition imposed on the core. Also, the study showed that the characteristic length used impacts directly the degree of correlation obtained, imminently improving the upscaling technique.

DEDICATION

I dedicate this thesis to my parents who have been a great source of inspiration, support, and their dedicated partnership for success in my life.

CONTRIBUTORS AND FUNDING SOURCES

Contributors

This work was supported by a thesis committee consisting of Assistant Professor Nayef Alyafei [advisor] and Associate Professor Albertus Retnanto of the Department of Petroleum Engineering and Professors Ahmed Abdel-Wahab and Mohammed Nounou from the Department of Chemical Engineering

Funding Sources

Graduate study was supported by a fellowship from Texas A&M University at Qatar and Faculty funding from Dr. Nayef Alyafei.

NOMENCLATURE

t_D	dimensionless time
k	permeability [mD]
ϕ	matrix porosity
L	core length, [cm]
V_B	bulk volume of the matrix block [cm^3]
A_i	surface area open to imbibition in the i-th direction [cm^2]
δ_{A_i}	distance from the open surface to the center of the matrix block [cm]
Q_w	cumulative water imbibed [m^3]
C	parameter that depends on the characteristics of the fluid-rock system [$m/\sqrt{s}$]
$F'(S_{wir})$	derivative of the capillary dominated fractional flow function at the irreducible water saturation.
D	capillary dispersion coefficient
F	capillary dominated fractional
$k_{ro\ max}$	maximum relative permeability of oil
$k_{rw\ max}$	maximum relative permeability of water
n	exponent for relative permeability of water curve shape
m	exponent for relative permeability of oil curve shape
S_w	water saturation

S_{wi}	initial Water saturation
S_{or}	residual oil saturation
k_{rw}	water relative permeability
k_{ro}	oil relative permeability
P_c	capillary pressure [Pa]
$P_{c\ entry}$	capillary pressure at the entrance of the pore throat [Pa]
F_s	shape factor
L_c	characteristic length [cm]
lA_i	distance traveled by the imbibition front from the open surface to the no-flow boundary[cm]
t	time [s]
t^*	early imbibition time [s]
tD	dimensionless time

TABLE OF CONTENTS

LIST OF FIGURES

Page

LIST OF TABLES

CHAPTER I

INTRODUCTION

1.1 Naturally Fractured Reservoirs

Due to the continued growth in hydrocarbon demand, petroleum engineers are facing the urge to drill deeper to uncover the untapped resources and enhance the productivity of existing reservoirs. It is estimated that naturally fractured reservoirs contribute to around 20% of the hydrocarbon reserves discovered worldwide (Saidi 1983). In such reservoirs, oil recovery is vastly improved when the appropriate recovery techniques are applied such as water flooding (Muggeridge et al., 2013). Moreover, these reservoirs are usually represented as dual porosity simulation models. This is because the porosity differs vastly between the matrix of the rock and the fracture itself, and so does the permeability (Warren and Root, 1963). Moreover, the irregular shape of the network of fractures is characterized by high permeability and porosity creating a heterogeneous medium in the reservoirs that permits more fluid to flow to the surface. Naturally fractured reservoirs are usually very difficult to characterize as engineers face hardships in predicting recovery from such systems (Gilman and Kazemi, 1983). Since the fractures act as a conduit for the fluid flow, the properties of the fluid vastly control the hydrocarbon recovery and hence making the physical interpretation of the process even more complex (Thomas et al., 1983). As the hydrocarbons flow from the low-perm matrix rock into the fracture conduit, spontaneous imbibition dominates. In specific, the oil stored in the pores of the matrix is mobilized by the means of capillary pressure or gravity (Gilman and Kazemi, 1988). This follows that saturating the matrix block with water will efficiently

displace the oil through forcing the water into the low permeability zone by the means of the difference in capillary forces. The illustration in **Figure 1** shows a fracture channel surrounded by the tight matrix block. The capillary forces push the oil from the pores of the rock into the flowing fracture carrying the hydrocarbon to the producer by the mean of water flooding. This variation in the saturation profile and the effect of the spontaneous imbibition process can be seen in the associated plot.

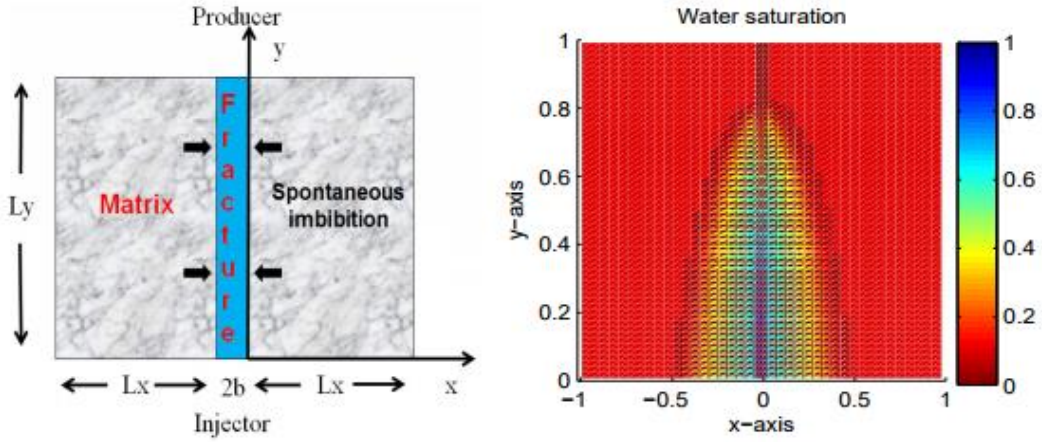

Figure 1 The fracture connecting an injector and a producer is shown (left). The oil is displaced due to spontaneous imbibition into the fracture which is then moved up to the producer by the water flow from the injector. This process is shown on a simulation grid depicting the change in the saturation profile along the fracture (right). (Andersen et al., 2013)

1.2 Research Problem

The petroleum literature lacks from detailed studies on numerical techniques of investigating spontaneous imbibition processes. Few papers discussed the steps of creating a base model to simulate counter-current imbibition assisted oil recovery and even fewer papers dealt with the upscaling of the numerical data into field dimensions while considering the different types of boundary conditions (Mason et al., 2009; Arabjamaloei & Shadizadeh, 2010; Nooruddin & Blunt, 2016). Most of the publishing authors try to validate their numerical solutions with experimental data that matches the same boundary condition. In fact, there is no research yet that involves numerical simulations covering the whole range of various boundary conditions and upscale data obtained without restrictions on the fluid properties of the flow.

On the other hand, numerical reservoir simulators are becoming essential in evaluating and predicting recovery from producing reservoirs nowadays. Such simulators can be problematic as they produce inaccurate results when the operating conditions are too complex. Researchers usually try to test the validity of the simulated results through comparing the numerical output of the simulator with mathematically developed analytical solutions (Nooruddin and Blunt 2016). In fact, the process of developing analytical solutions for imbibition is not an easy task as the flow is highly non-linear. Therefore, the need for scaling laws emerge in order to reduce the differences in fractional recovery between different imbibition processes with varying operating conditions.

1.3 Objectives

The goal of this research is to construct a base matrix block simulation model in Eclipse 100 black oil commercial Schlumberger simulator governing a 1-D, 2-D and 3-D flow. Different boundary conditions resembling the wetting phase of reservoir rocks will be imposed to the simulated model and the effects of the characteristic length - a parameter that accounts for different boundary conditions to compensate for the geometry of the matrix elements applied to reservoirs - per case will be evaluated. The idea behind varying the characteristic length is to show the effect of the boundary conditions on oil recovery. The results of oil recovery from the different simulation runs will be upscaled to field dimensions and compared with the analytical solution suggested by Schmid et al. (2011, 2016). A detailed parametric study will then follow to investigate the effect of the operating parameters on the validity of the Schmid and Geiger (2012) scaling group. The study addresses the importance of employing simulation techniques to predict flow properties that rather seem difficult to produce through routine laboratory tests.

CHAPTER II

FUNDAMENTALS

2.1 Capillary Pressure

Capillary pressure – P_c – is defined as the difference in fluid pressure across an interface between two fluids in a confined volume. The intermolecular forces acting on two immiscible phases (eg. oil and water) cause each phase to contract to a minimal state resulting in a curved interface between the two miscible fluids. Capillary pressure is usually the difference between the pressure of the non-wetting phase and the pressure of the wetting phase as follows (Anderson, 1986):

$$P_c = p_{non-wetting-phase} - p_{wetting-phase} \qquad \textbf{(2.1)}$$

This equation can be translated in term of the fluids in an oil-water system to be

$$P_c = p_w - p_o = \Delta p = \frac{2\sigma}{r} \qquad \textbf{(2.2)}$$

Where:

- p_w is the pressure of the water (non-wetting phase) in Pa
- p_o is the pressure of the oil (wetting phase) in Pa
- σ is the interfacial tension between the two phases N/m
- r is the radius of the pore throat in m.

In a capillary tube, forces are always in equilibrium when balanced on any segment if the interface itself is in equilibrium. The oil- water system presented in **Figure 2** relates

the capillary forces in a tube to the height of the fluid rise (Amyx et al., 1960) through this relation:

$$P_c = p_w - p_o = (\rho_w - \rho_o)gh \qquad \textbf{(2.3)}$$

Where ρ_o and ρ_w are the oil and water densities in kg/m^3 respectively; g is the acceleration due to gravity m/s^2, and h is the height of the column of water in the capillary tube with respect to a reference point in m.

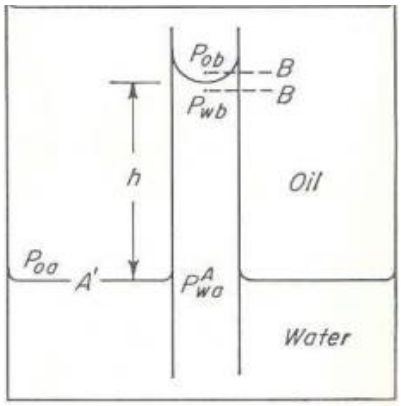

Figure 2 Schematic diagram representing capillary pressure difference between the oil and water phases (Clark, 1997)

The capillary forces are fundamental in driving the pressure during spontaneous imbibition. This pressure subsequently forces the wetting phase to flow out of the rock pores through displacing it by the non-wetting phase. In simple words, the process is an elemental mass balance. If we assume that a rock is preferentially water wet, then water tends to rise inside the pore due to the capillary difference between the water and oil phases. In order to displace the water, an equivalent pressure to the capillary must be applied. In this way, water is forced to leave the rock; the bigger the pore the, lower the required capillary pressure is and the opposite is true.

The capillary pressure curve depends greatly on Drainage and Imbibition process. Drainage is defined by an increase in the saturation of the non-wetting phase thus increasing the mobility of the non-wetting phase in return. On the other hand, imbibition is characterized by an increase in the saturation of the wetting phase thus increasing wetting fluid phase mobility.

These phenomena can be explained in a capillary pressure curve plotted against water saturation in a rock. Observing **Figure 3**, the imbibition curve shows a tendency of the wetting phase to naturally saturate the rock. This process resembles waterflooding an oil reservoir in which the reservoir is water-wet. Drainage curve is also shown in green.

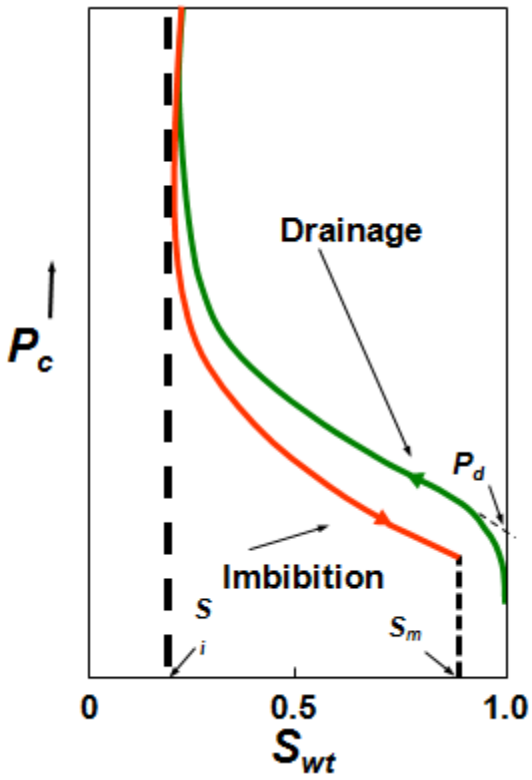

Figure 3 Typical imbibition curve in a core sample (Petropedia.com)

2.2 Wettability

Wettability is the tendency of one fluid to spread on or adhere to a solid surface in the presence of other immiscible fluids. The wettability of the formation is an essential factor to optimize the recovery from oil reservoirs. Its importance lies in the influential effect that it plays in waterflooding and enhanced oil recovery techniques through wettability alteration processes. Wettability is simply the interfacial interaction between fluid and solid phases (Robin, 2001). Let us say that we drop a non-wetting fluid onto a surface covered by the wetting fluid, the drop will try to minimize its contact with the surface forming a solid round droplet. The balance of forces exerted on the droplet and the surface creates an angle theta between the droplet and the solid surface, and thus defining the condition of the wetting phase. The measurement of the contact angle in the lab helps in determining the state of the wettability of the rock. In general, if the angle theta is between 0^o and 90^o, the rock is preferentially water wet. On the other hand, the rock is said to be oil-wet if the contact angle is between 90^o and 180^o. The schematics in **Figure 4** below shows the two-wetting cases discussed earlier.

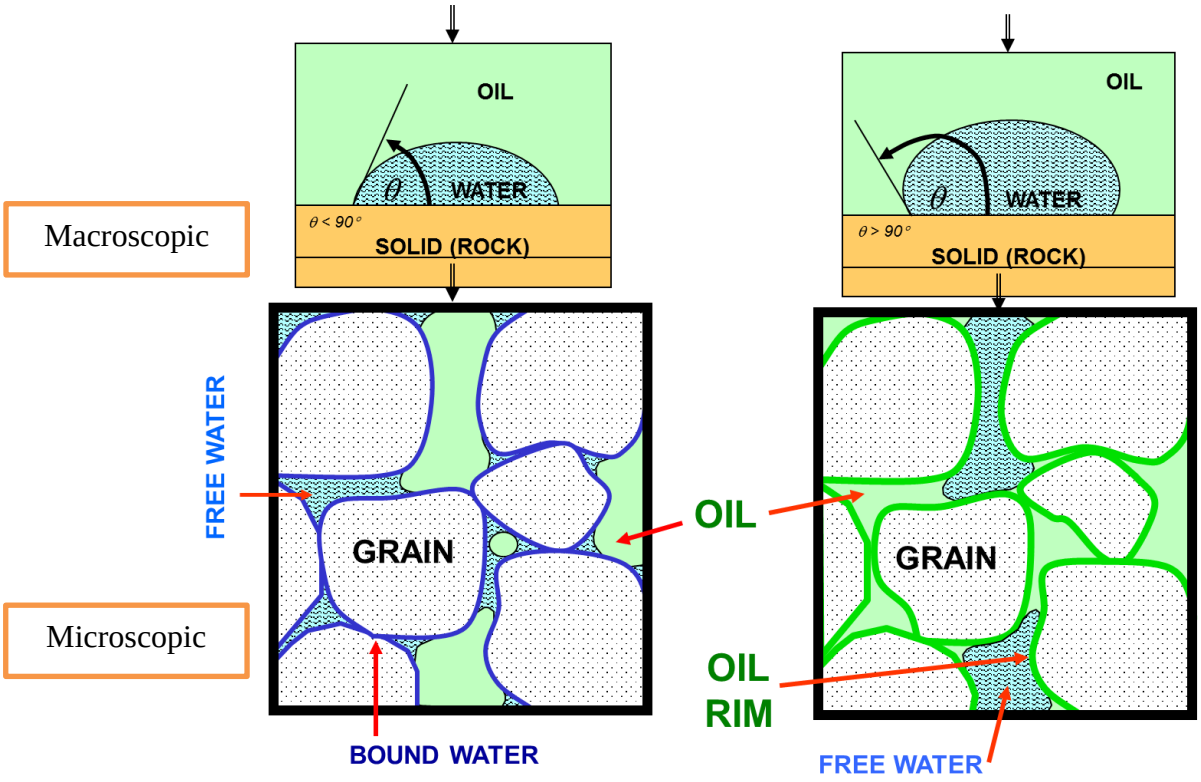

Figure 4 The illustration shows the microscopic porous structure of the core and the measurement of the contact angle for oil-wet (right) and water-wet (left) systems. (Modified from Fekete.com).

Additional wettability classifications can be:

1- Neutral wettability where there is preferential to neither of the fluids present in the pores.

2- Fractional wettability where the reservoir is mainly water-wet with local areas of oil-wet states. The small pores are filled with water while the bigger pores are filled with oil. This case can be experienced in rocks where residual oil saturation is low.

2.3 Relative Permeability

The simultaneous flow of the wetting and a non-wetting phase together in a porous media is greatly affected by the wetting state of each phase and their respective relative permeabilities. The relative permeability defines the distinct path for a fluid to follow inside a reservoir rock as well as its flow capability. The mobility of such fluid depends mainly on the pore geometry, wettability, fluid distribution and fluid saturation. Mathematically, relative permeability can be defined as the ratio of effective permeability - The ability to preferentially flow or transmit a particular fluid when other immiscible fluids are present in the reservoir - of a specific fluid at a constant saturation to the absolute permeability - the measurement of the permeability conducted when a single fluid or phase is present in the rock - of the rock where this fluid flows.

Ideally, relative permeability is measured through core samples in lab tests. However, such tests are time-consuming and expensive to perform. If we consider a water-oil system in a reservoir rock, 4 distinct relative permeability curves could exist:

1) Water - wet systems
2) Oil - wet systems
3) Mixed wet systems
4) Intermediate wet systems

In reservoir rocks, the sum of the relative permeability values of the different phases available should always be less than one. **Figure 5** below depicts an oil-water system for

a water-wet rock. In water-wet rocks, a thin immobile film of water form on the outer frame of the pores and acts like a lubricant the non-wetting phase. The water starts from a point S_{wc} which we call the connate or irreducible water saturation. At this point, water is immobile due to the capillary forces acting the pores and hence the respective relative permeability for water is zero. Conversely, the oil will have a maximum relative permeability that starts to decrease with increasing water saturation until the residual oil saturation is reached (S_{or}). Beyond this point, the oil will be immobile and thus its relative permeability will be zero. The water relative permeability will be at its peak when critical oil saturation is reached. It can be observed from the **Figure 5** that the intersection between the relative permeability curve of oil and water shifts towards the right indicating a water-wet system. On the other hand, this intersection is noticed to shift to the left in oil-wet rocks while having water relative permeability curve much higher than that of oil (**Figure 6**).

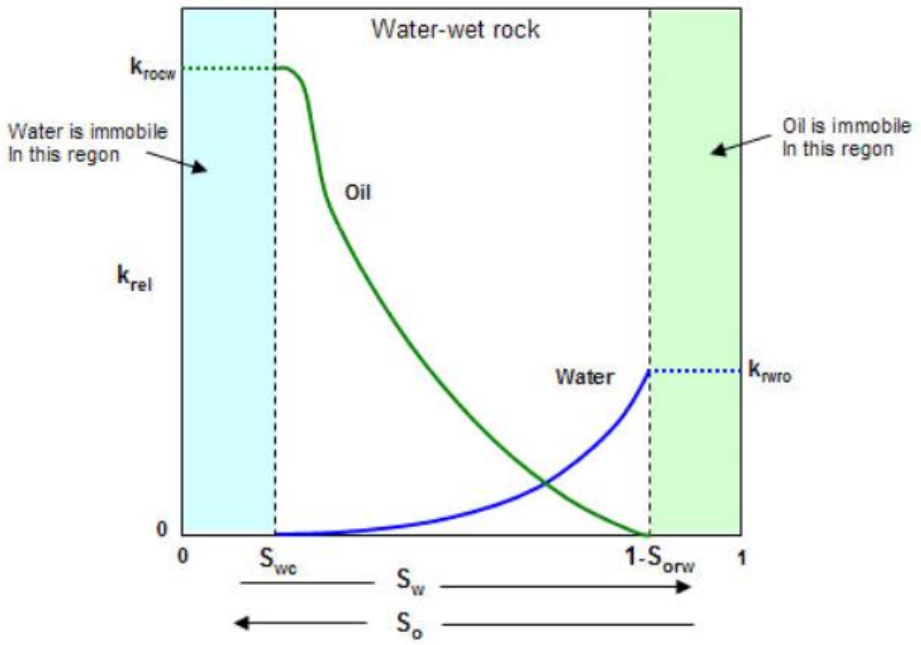

Figure 5 Typical Relative permeability curve in a water-wet rock (Adapted from Fekete.com).

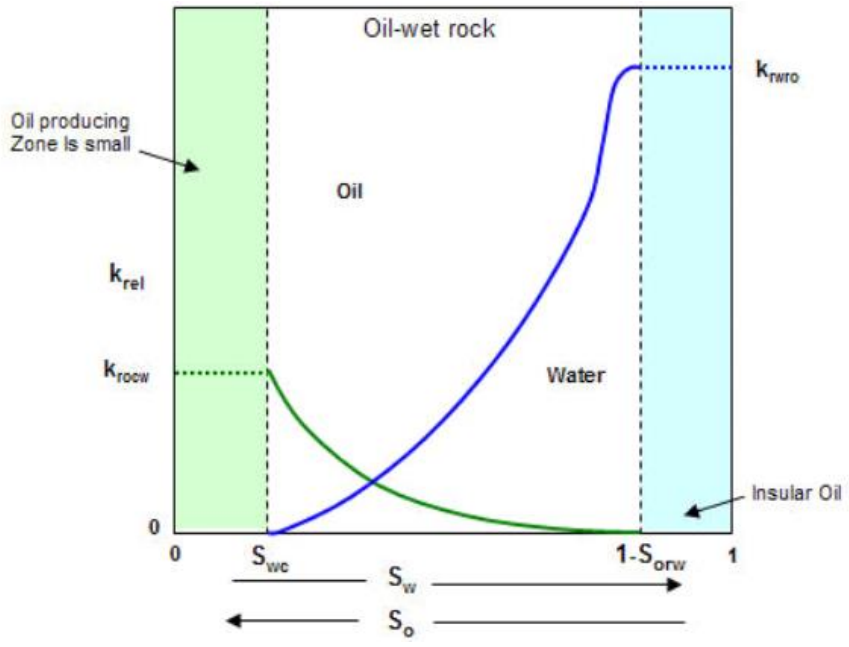

Figure 6 Typical Relative permeability curve in an oil-wet rock (Adapted from Fekete.com).

2.4 Spontaneous Imbibition

The physical phenomenon of imbibition is important in the understanding of fluid flow in water drive reservoirs as it directly affects water movement and areal sweep efficiency (Meng et al., 2016). Imbibition is scientifically defined as the absorption of a-wetting phase into a porous rock and can be divided into two main categories: forced and spontaneous (Ge et al., 2015). In our everyday life, we dry dishes using paper towels, or we write on a sheet of paper using ink. The physical transfer of the water into the paper towels or the ink onto the sheet of paper is described as spontaneous imbibition (SI) (Mason and Morrow, 2001). The fluid imbibes into the porous structure of the paper towel or the sheet of paper due to capillary forces. In petroleum terms, SI is when oil (non-wetting phase) in a reservoir is displaced by water (wetting phase) with no pressure driving the water phase into the rock. The process is driven by the difference in the capillary force as the spontaneous imbibition recovery is higher when the hydrophilicity of the rock surface is stronger (Huang et al., 2015). Different rock and fluid properties such as permeability, wettability and interfacial tension between the wetting and the non-wetting phase determine how fast the non-wetting phase would move out of the rock to be replaced by the wetting phase (Anderson, 1986).

The most common forms of spontaneous imbibition are called co-current and counter current in which the fluid phases flow in identical and opposite directions respectively. In both cases, the boundary conditions have a great effect on the imbibition rate (Hamon and Vidal 1986). In co-current flow, the water flows from one end of the rock pushing the oil towards the opposite end. On the other hand, counter-current flow involves

only one open flow boundary with the rest of the boundaries isolated and sealed. Both the wetting and the non-wetting phase flow in and out respectively from the same end.

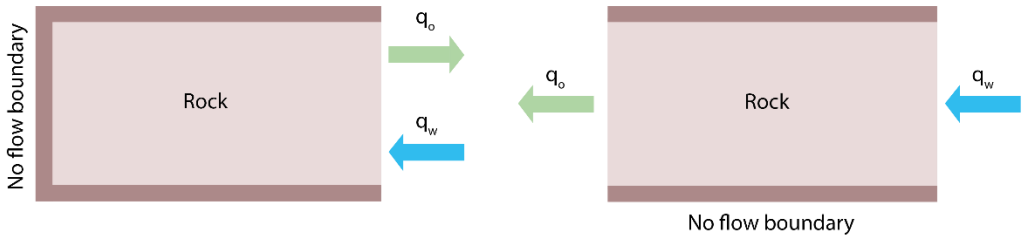

Figure 7 The illustration on the left shows counter-current spontaneous imbibition, while the illustration on the right shows co-current spontaneous imbibition of an oil-water system in a water-wet rock (Khan and Alyafei, 2018)

CHAPTER III

BACKGROUND AND LITERATURE REVIEW

This chapter details the early efforts to scale oil recovery with dimensionless time experimentally and analytically for spontaneous imbibition processes.

3.1 Transfer Functions

The mathematical definition of a transfer function has been of great benefit to the advance of modern science. Laplace transformation is one type of transfer functions relating the output and the input of the system through a ratio than can be denoted by G(s). Let us imagine our transformation process as a simple magic box. A function U(s) goes into one end of the box and undergoes a Laplacian transformation to yield Y(s) at the other end. Thus, a transfer function could be defined as G(s) = Y(s)/U(s).

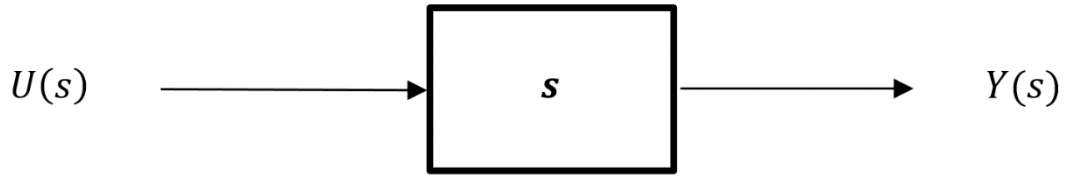

Figure 8 Schematic representation of Laplace transfer function.

3.1.1 Scaling Transfer Fucntions

In petroleum engineering, transfer functions are widely used in scaling processeses to predict oil recovery in reservoirs from lab experiments. Scaling transfer functions can be used in the representation of fracture-matrix systems to increase the efficency of oil recovery predictions from field simulators (Mason and Morrow, 2001).

Extensive research has been done in the past to understand the phenomenon of spontaneous imbibition in water-wet rocks and to scale experimental data of oil recovery (Iffly et al., 1972; Du Prey, 1978; Hamon and Vidal 1986; Bourbiaux and Kalaydjian, 1990; Cuiec et al., 1994; Zhang et al., 1996; Cil et al., 1998; Rangel-German and Kovscek, 2002). Upscaling imbibition assisted oil recovery as a function of dimensionless time has been of great importance to the researchers and was exhibited through the development of various scaling groups (Standnes, 2010). Such scaling groups can greatly facilitate the process of predicting oil recovery from the reservoirs. In other words, lab tests done on rock samples can be used to estimate macro-level oil recovery of a reservoir when integrated into field-scale simulators.

3.2 Early Scaling Groups

Many authors have proposed various scaling groups to correlate imbibition data since 1918. One of the earliest equations developed was that of Lucas and Washburn (1918) describing a counter-current spontaneous imbibition flow. The equation of the dimensionless time proposed:

$$t_D = \frac{1}{2}\frac{1}{L^2} r \frac{\sigma}{\mu_w} t \qquad \textbf{(3.1)}$$

where *r* is the tube radius and *L* is the tube length. This equation was of a vital importance since it shows the pace of the imbibition progression; it starts very fast at preliminary stages then slows down intensely.

After that, Mattax and Kyte (1962) proposed a modified scaling group based on the work of Rapoport (1995). In their work, Mattax and Kyte (1962) performed flow tests in 1-D and 3-D systems. However, a critical limitation of their experiments is that the connate water saturation was not accounted for in the tests. Realistically, initial water saturation is present in the full-scale reservoirs, and hence discrepancies could be expected when scaling from the core to the field if this model is used. These tests allowed for the prediction of the following scaling group

$$t_D = \sqrt{\frac{k}{\phi}} \frac{1}{L^2} \frac{\sigma}{\mu_w} \, t \qquad \textbf{(3.2)}$$

where t_D is dimensionless time, k is permeability, ϕ is matrix porosity, σ is interfacial tension, μw is water viscosity, L is characteristic length, t is imbibition time

To achieve a good measure of correlation between the experimental data and that predicted by the scaling group, Mattax and Kyte (1962) imposed many limitations;

i. The geometric shape of the reservoir and the core sample has to be consistent.
ii. The initial fluid saturation has to be the same in both field and lab data.
iii. The water/oil viscosity ratio should be similar in both laboratory and reservoir system
iv. The relative permeability profiles used in the lab should match those in the reservoir block.

Although this work could be considered a decent starting point to scale up imbibition recovery, other scaling groups with less number of imposed limitations are needed to achieve a high level of accuracy.

Reis and Cil (1993) utilized the mass balance equation together with Darcy equation to come up with a scaling group for linear imbibition represented by:

$$t_D = \frac{1}{L^2}\sqrt{\frac{K}{2\phi}}\frac{1}{\Delta S_w}\frac{\sigma}{(\frac{\mu_w}{0.1}+\frac{\mu_{nw}}{0.1})}t \qquad \textbf{(3.3)}$$

This model included the mobility of the both displacing and displaced fluids, a factor in which Mattax and Kyte (1962) failed to represent.

3.3 Characteristic Length and Shape Factor

Later follows the work of Ma et al. (1997) where a shape factor that accounts for different boundary conditions was identified. Ma et al. (1997) based their work on the shape factor derived by Kazemi et al. (1992) reflecting the effect of diverse boundary conditions in a rock sample :

$$F_s = \frac{1}{V_B}\sum_{i=1}^{n}\frac{A_i}{\delta_{A_i}} \qquad \textbf{(3.4)}$$

where V_B is the bulk volume of the matrix block, A_i is the surface area open to imbibition

in the i-th direction, δ_{A_i} is the distance from the open surface to the center of the matrix block, and n is the total number of surfaces open to the imbibition

Based on the equation of the shape factor, a characteristic length, Ls, was readily formulated:

$$L_s = \frac{1}{\sqrt{F_s}} = \sqrt{\frac{V_B}{\sum_{i=1}^{n} \frac{A_i}{\delta_{A_i}}}} \qquad \textbf{(3.5)}$$

Combining the knowledge gained from developing the aforementioned equations, Ma et al. (1997) proposed a modified equation for the character length based on Kazemi and Hamon and Vidal (1986) work:

$$L_c = \sqrt{\frac{V_B}{\sum_{i=1}^{n} \frac{A_i}{l_{A_i}}}} \qquad \textbf{(3.6)}$$

where A_i is the distance traveled by the imbibition front from the open surface to the no-flow boundary

Moreover, Ma et al. (1997) derived a new dimensionless time that utilizes the characteristic length and depends on an empirical factor that is easily measured; the square root of the product of the viscosities of the wetting and the non-wetting phases.

The equation can be represented by:

$$t_D = \frac{1}{{L_c}^2}\sqrt{\frac{K}{\phi}}\frac{\sigma}{\sqrt{\mu_w \mu_{nw}}}t \qquad \textbf{(3.7)}$$

The equation was able to match all the available imbibition data back then without imposing various restrictions on the input values. However, this equation suited oil/water/rock systems under a set of conditions including that wettability, and relative permeability curves must be identical, the initial fluid distribution must be duplicated, and gravity effects are negligible. These limitations raised many questions about the usability of this scaling group.

In fact, the relative permeability plays a critical role in imbibition analysis, and hence Zhou et al. (2002) and Li and Horne (2004) managed to include those parameters in the dimensionless time equation. However, their work was limited to gas/water/rock systems because of the assumption that the mobility of the non-wetting phase is infinite. Never the less, the subsequent efforts of Li and Horne (2006) enabled the development of another equivalent scaling method that works for the oil/water/rock systems while considering the relative permeabilities of both: the wetting and the non-wetting phases. The Li and Horne (2006) equation are expressed as follows:

$$t_D = c^2 \frac{k k_{re}^*}{\phi}\frac{P_c^*}{\mu_e}\frac{S_{wf}-S_{wi}}{{L_a}^2}t \qquad \textbf{(3.8)}$$

This model works surprisingly well for both co-current and counter-current spontaneous imbibition cases.

3.4 Modified Scaling Group

Recently, a new scaling group was derived by Schmid et al. (2012) based on the general, exact solution of the two-phase Darcy equation for the case of counter-current imbibition (McWhorter and Sunada, 1990). This model is considered as the 'master equation' for scaling spontaneous imbibition where all previously derived models appear to be special cases of this generic model:

$$t_D = \left[\frac{Q_w(t)}{\phi L_c}\right]^2 = \left[\frac{2C}{\phi L_c}\right]^2 t \qquad \textbf{(3.9)}$$

This equation is unique as all assumptions were relaxed when deriving the model except for those applicable to Darcy's law, and it states the total volume of the wetting phase imbibed characterizes Spontaneous imbibition systems.

In their paper, Schmid and Geiger (2012) clarified that the derived solution is only valid on the basis that the wetting front has not reached the end of the core or hindered any other water front is moving from further exposed surface areas. The time t^* represents the end time in which the analytical solution stops being valid as in late times the model severely fails in predicting the slowdown in recovery rates. This time t^* is called "early-time imbibition" and is represented by:

$$t^* = \left[\frac{L\phi}{2CF'(S_{wir})}\right]^2 \qquad \textbf{(3.10)}$$

where $F'(S_{wir})$ is the derivative of the fractional flow function at the irreducible water saturation. The table below presents a summary of the scaling groups discussed earlier.

Table 1 A summary of the main scaling groups devised to model spontaneous imbibition

Author	Dimensionless time	Comments
Lucas and Washburn (1918,1921)	$t_D = \frac{1}{2}\frac{1}{L^2} r \frac{\sigma}{\mu_w} t$	This model predicted that the cumulative volume imbibed is proportional to the square root of time. However, it is invalid in cases where gravity force is dominating and high permeability zones.
Mattax and Kyte (1962)	$t_D = \sqrt{\frac{K}{\phi}} \frac{1}{L^2} \frac{\sigma}{\mu_w} t$	The model was based in Darcy's law to develop a scaling group for two-phase flow. The equation imposes restrictions on the core shape, relative permeability, viscosity ratios, effect of gravity and capillary pressure profile. On the other hand, this analysis help understands recovery behavior from fracture-matrix, water drive reservoirs.
Reis and Cil (1993)	$t_D = \frac{1}{L^2} \sqrt{\frac{K}{2\phi}} \frac{1}{\Delta S_w} \frac{\sigma}{(\frac{\mu_w}{0.1} + \frac{\mu_{nw}}{0.1})} t$	This model scales linear imbibition profiles for two-phase flow. It was developed through combing Darcy law and mass balance. In fact, the scaling groups was based on the first simple, closed-form, analytical model that incorporates the key petrophysical properties without any empirical parameters. However, many assumptions have been made in the development of this model limiting its applicability.
Ma et al (1997)	$t_D = \frac{1}{{L_c}^2} \sqrt{\frac{K}{\phi}} \frac{\sigma}{\sqrt{\mu_w \mu_{nw}}} t$	This model incorporated new definition of the characteristic length and a viscosity ratio term enabling the scaling of imbibition oil recovery data for different core sizes, boundary condition, and oil and water viscosities against dimensionless time. However, this equation can only predict the behavior of strongly water-wet systems.
Li and Horne (2006)	$t_D = c^2 \frac{k k_{re}^*}{\phi} \frac{P_c^*}{\mu_e} \frac{S_{wf} - S_{wi}}{{L_a}^2} t$	This model is considered the first general scaling group for different rock systems in both counter-current and co-current imbibition. It was developed based on a thorough theoretical analysis of fluid-flow mechanisms. Nevertheless, measuring the parameters governing the flow and the rock properties in the lab is time consuming and expensive, hence causing a severe set-back to the feasibility of this model.

Table 1 Continued

Author	Dimensionless time	Comments
Schmid and Geiger (2012)	$t_D = \left[\frac{Q_w(t)}{\phi L_c}\right]^2 = \left[\frac{2C}{\phi L_c}\right]^2 t$	This model accounts for the effect of all flow and rock properties on spontaneous imbibition where it serves as the master equation for scaling imbibition recovery. It works well with water-wet and mixed-wet cases, and characterizes SI by the cumulative inflow without the need of any fitting parameters. However, this model ignores viscous and gravity forces and is only valid for a certain time range where $t < t^*$.

CHAPTER IV

NUMERICAL MODELLING OF SPONTANEOUS IMBIBITION PROCESS

In this chapter, we will discuss the steps to build a numerical 2-D model for a water-wet core sample. This model will be used to simulate counter-current spontaneous imbibition based on the input parameters provided in Schmid et al. (2016) study and then this is compared with the analytical model of Schmid et al. (2011). We will then construct the relative permeability and capillary pressure curves based on power-law model and perform a sensitivity study with regards to the grid side of the simulation model.

4.1 Analytical Solution for Co-current and Counter-current Spontaneous Imbibition

The relative permeability and capillary pressure curves were obtained for the studied rock and used in the analytical solution for co-current and counter-current spontaneous imbibition developed by Schmid et al. (2011). The analytical solution for spontaneous imbibition utilizes the fractional flow theory for viscous-dominated flow where displacement is controlled entirely by capillary forces. The model is initiate through a simple mass balance for two phase flow. Using Darcy's Law, and ignoring gravitational forces and capillary back pressure, the derivation leads to the following two analytical solutions for the co-current and counter-current imbibition case respectively as follows:

$$(F - f)F'' = -\frac{\phi}{2C^2}D \qquad \textbf{(4.1)}$$

$$FF'' = -\frac{\phi}{2C^2}D \qquad \textbf{(4.2)}$$

where *D* is the capillary dispersion coefficient defined as $D(S_w) = -\frac{k\lambda_w\lambda_{nw}}{\lambda_t}\frac{dP_c}{dS_w}$, *F* is the capillary dominated fractional flow function and *C* is an empirical constant $[\frac{m}{\sqrt{s}}]$

In order to solve for *C* and *F*, one would have to solve the integral implicitly. However, a simple excel program utilizing the concept of backward-differencing approximation through an iterative process of the unknown constant *C* is used (Schmid et al., 2016 and Alyafei et al., 2016). This excel sheet makes use of the following equations:

$$F(S_{wir}) = 0 \qquad \textbf{(4.3)}$$

$$\sum_{i=1}^{n} F'(S_w, i)\,.\,\Delta S_w \;\approx\; \frac{Q_w(t)}{\phi} = \frac{\phi}{2C\sqrt{t}} = 1 \qquad \textbf{(4.4)}$$

The solution process is as follows:

1- Determine *F"* from a backward-differencing approximation

2- Iteratively determine $F(Sw)$ at a finite number *n* of saturation points

3- Iterate on the constant *C*.

4- Keep changing *C* until $F(Sw)$ converges to the correct solution

The final value of *C* is obtained when **Eq. 4.3** converges to 0, and **Eq. 4.4** converges to 1.

4.2 Building the Grid Model

Based on Schmid et al. (2016) data, a strongly water-wet state case was used to serve as the basis of the numerical simulation with four different boundary conditions, which will be discussed later. The core was modeled as a rectangular prism of 7.66 cm ×2.5 cm ×2.5 cm dimensions. Furthermore, the model represents a conventional single porosity (20%) and single permeability (300 mD) rock sample that utilizes Cartesian gridding for property distribution.

The simulation model was developed on a commercially available black oil simulator. The number of grids used is finite in order to approximate the volume of the core. This finite number will allow us to solve the flow equations in a numerical fashion. Subsequently, the most efficient number of grids in the shortest simulation time possible was determined by performing a sensitivity analysis. For this purpose, a rectangular grid was created mimicking a one end open flow boundary in which all the sides of the core are sealed and isolated except for one end. An extra gridblock was attached to the open end of the core to serve as a water tank for the imbibition process with an equivalent volume of 10 times that of the core pore volume. The water tank was set to have 100% water saturation and porosity.

4.3 Input Parameters

The relative permeability curves were constructed based on the power law model:

$$k_{rw} = k_{rw\,max}\left[\frac{S_w - S_{wi}}{1 - S_{wi} - S_{or}}\right]^n \qquad \textbf{(4.5)}$$

$$k_{ro} = k_{ro\,max}\left[\frac{1 - S_w - S_{or}}{1 - S_{wi} - S_{or}}\right]^m \qquad \textbf{(4.6)}$$

where $k_{ro\,max}$ is the maximum relative permeability of oil, $k_{rw\,max}$ is the maximum relative permeability of water, *n* and *m* are the relative permeability exponents, S_w is the water saturation, S_{wi} is the initial water saturation, S_{or} is the residual oil saturation, k_{rw} is water relative permeability and k_{ro} is the oil relative permeability.

On the other hand, the capillary pressure prediction model in a water-wet system follows the following relation

$$P_c = P_{entry}\left[\frac{S_w - S_{wi}}{S_{w\,@\,Pc\,entry} - S_{wi}}\right]^l \qquad \textbf{(4.7)}$$

P_c is the capillary pressure, $P_{c\,entry}$ is the capillary pressure at the entrance of the pore throat, and $S_{w\,@\,Pc\,entry}$ is the water saturation at the $P_{c\,entry}$.

The generated relative permeability and capillary pressure plots are presented in **Figure 9** and **Table 2** summarizes the input parameters used to calculate the analytical solution for a strongly water-wet case based on Schmid et al. (2016) data. . The analytical solution for this specific case returned a *C* value of 4.63×10^{-5} $[\frac{m}{\sqrt{s}}]$

Table 2 Parameter sets representing a strongly water-wet Brea sandstone referenced in Schmid et al. (2016) and used to solve for the counter current analytical model the analytical solution.

Parameter	**Value**
S_{wi}	0.2
S_{or}	0.4
$k_{rw\ max}$	0.2
n	3
$k_{ro\ max}$	0.85
m	1.5
P_{entry} [Pa]	12000
l	-0.7
μ_w [cP]	1
μ_o [cP]	3
ϕ	0.2
K [mD]	300

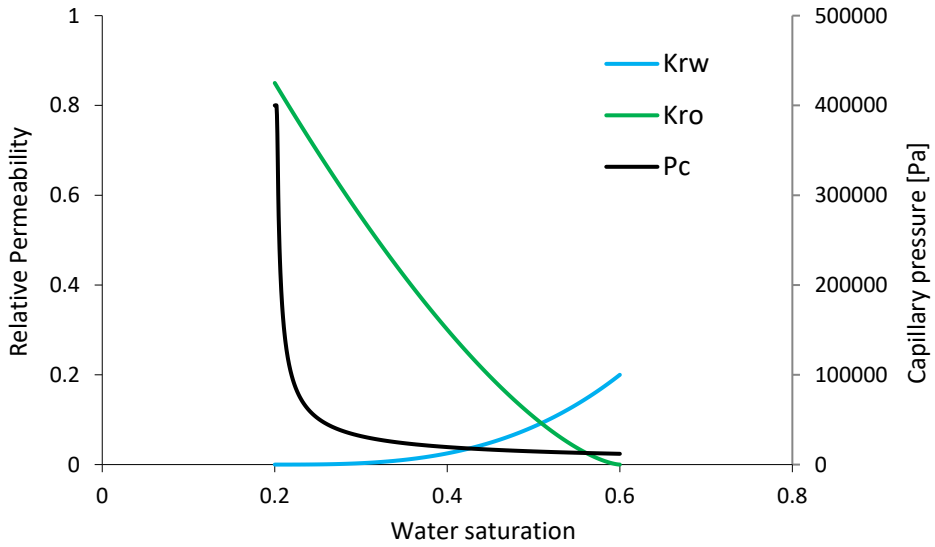

Figure 9 Capillary pressure and relative permeability for a strongly water-wet sandstone rock. The green color refers to the oil while the blue color refers to the water

4.4 Discretization of the Model and Grid Sensitivity Analysis

After creating the model, the dimensions of the Cartesian grid were varied in six intervals and are shown in **Table 3**. The plots of oil recovery as a function of time and the CPU time required to perform the simulation runs were the most influential factors in determining the optimal number of grids to be used in our model. It can be interpreted from **Figure 10** that as the number of grids used becomes larger, the discrepancies in the oil recovery curves diminish. If we examine grid 50×50×1 and grid 100×100×1 closely, we can see that the two curves are almost overlapping compared to previous coarser grids. To quantify the difference in the results of cases 5 and 6, the mean squared error was calculated. Mean square error (MSE) is probably the most commonly used error metric (McLean et al., 2012). It penalizes more substantial errors because squaring larger numbers has a more significant impact than squaring smaller numbers. The MSE calculation in our case returned a rather small number of 0.00258 %. Hence, the cutoff for the grid size is deduced to be a 50×50×1 grid size.

Furthermore, the simulation time to run each of the six cases was recorded in **Table 3.** The time to simulate the first 3 cases in which a relatively coarse grid was used is almost the same averaging at 5.87 seconds. As a finer grid is simulated, CPU time started to increase exponentially reaching a value of 108 sec for run six where a 100×100×1 grid size is used. The running time to solve the pressure equation in a finer gridblock is quite large, compared to the time taken to simulate a grid size of 50×50×1 at around 33 seconds.

As a final validation step for the applicability of our simulation model, we plotted the analytical solution corresponding to the same properties used in the simulation file. The black line representing the analytical solution is observed to match the finer grid block sizes at early times where the analytical solution is valid. Hence, we can say with confidence that the threshold of 50×50×1 grid size is critical where any larger grid would take much more time to simulate without any significant return on the accuracy of the results. This choice of grid size guarantees the convergence of the simulation results in a fashionably timed manner.

Table 3 Table of grid sizes investigated in the grid sensitivity analysis.

Case	**Number of gridblock in I, J, and J**			**Total Number of grid blocks**	**CPU Time (sec)**
	I-direction	**J-direction**	**K-direction**		
1	7	7	1	49	5.65
2	10	10	1	100	5.82
3	15	15	1	225	6.15
4	20	20	1	400	16.48
5	50	50	1	2500	33.52
6	100	100	1	10000	108.11

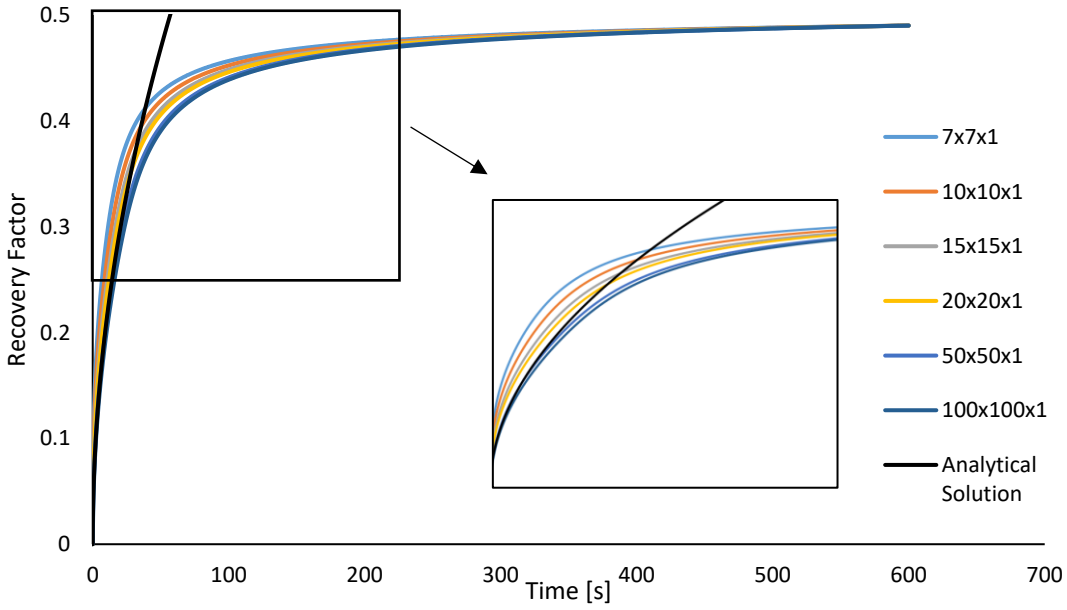

Figure 10 The graph shows the oil recovery factors for different grid sizes. The effect of the grid size is clear from the results of the static imbibition runs.

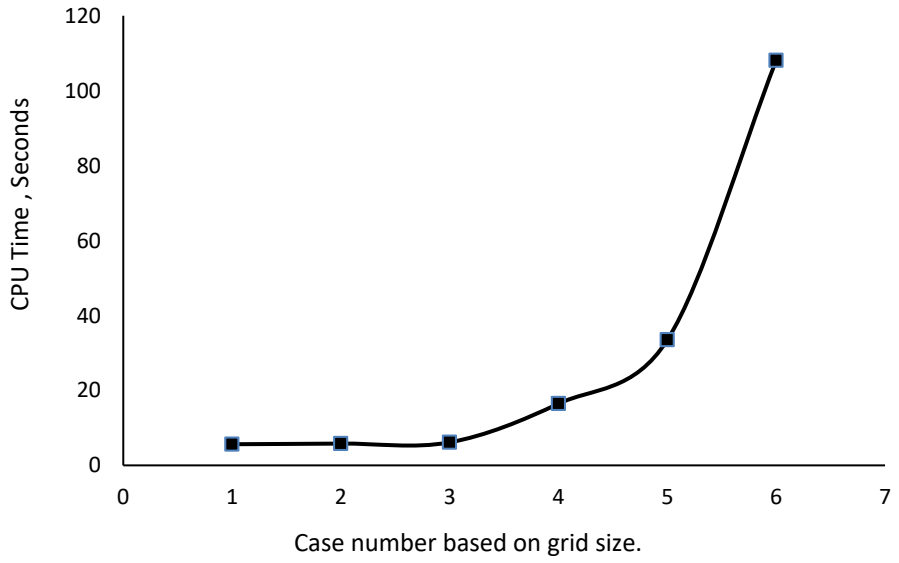

Figure 11 CPU time required to converge to a solution for each grid size. The time increases exponential with grid numbers used

4.5 Boundary Conditions and Characteristic Length

Once the 50×50×1 model has been established, different boundary conditions scenarios were considered. The volume of water imbibed from the water tank into the rock sample was used to predict the recovery factors for each boundary condition studied.

The following boundary conditions were studied in the counter-current simulation case (Yildiz et.al, 2006):

a) One End Open (OEO) is when the different sides of the core sample are isolated permitting the wetting phase to flow into the core through one open end located at the left side of our horizontal core.

b) Two Ends Open (TEO) is when the top and the bottom sides in the i-direction of the core are isolated while the flow occurs throughout the whole length of the core.

c) Two Ends Closed (TEC) is when the wetting phase flows into the rock through the top and the bottom sides while isolating the entire length of the core sample

d) All Faces Open (AFO) is when all sides of the core are exposed to the flow imbibing the wetting phase into the pores of the core sample.

During the imbibition assisted oil recovery phenomenon, the rate of oil recovered is significantly affected by the geometric elements of the matrix including the size, shape and boundary conditions applied to the core sample.

Therefore, Schmid and Geiger (2012) used the characteristic length to represent different boundary conditions when scaling the SI data. Moreover, **Eq. 3.6** will be used in this section to represent the different boundary conditions shown in **Figure 12**. Moreover, **Table 4** shows a summary of the formulas used to calculate the shape factor and the characteristic length for a rectangular prism (**Figure 13**) representing our core for the four boundary conditions: OEO, TEC, TEO, and AFO as in a, b, c and d respectively.

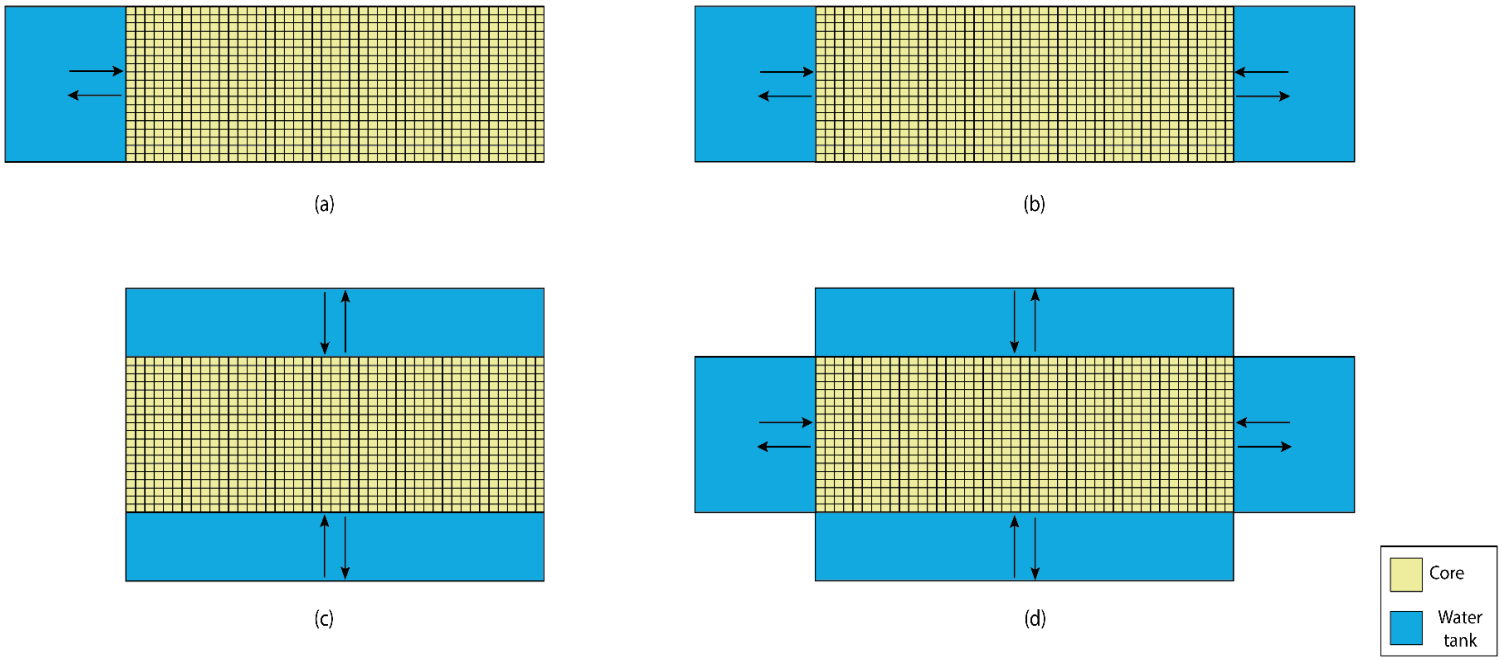

Figure 12 Schematic representation of the different boundary conditions considered in this study

Table 4 Shape factors and characteristic lengths of a rectangular prism similar to the one shown in figure 12 with different boundary conditions (Cesur et al., 2006).

Boundary Condition	$F_{s,}(cm^{-2})$	$L_{c,}(cm)$
AFO	$\frac{4}{L^2}+\frac{8}{a^2}$	$\frac{aL}{2}\sqrt{\frac{1}{a^2+2L^2}}$
TEC	$\frac{8}{a^2}$	$\frac{a}{2\sqrt{2}}$
TEO	$\frac{4}{L^2}$	$\frac{L}{2}$
OEO	$\frac{1}{L^2}$	L

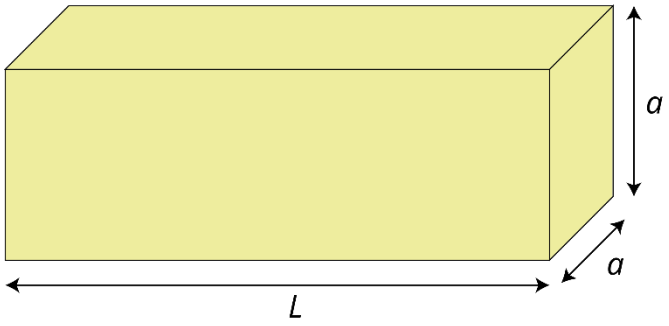

Figure 13 Dimensions for a rectangular prism core sample

CHAPTER V

SCALING OF SPONTANEOUS IMBIBITION MECHANISM

In this chapter, the numerical results of the simulation obtained through the simulation model discussed in the previous chapter have been upscale to field dimensions with a varying set of boundary conditions. Moreover, the validity of the scaling group and the characteristic length imposed has been assessed along with the analytical solution for spontaneous imbibition.

5.1 Comparison of Oil Recovery Time with Different Boundary Conditions

In general, the amount of recovered oil will increase as the number of faces available for imbibition increases. In order to verify this statement, we plotted the recovery of oil versus time for the different boundary conditions tested: OEO, TEO, TEC, and AFO **(Figure 14)**. The highest recovery at around 52% was achieved when all the faces of the core were exposed to water thus enhancing the counter-current imbibition process. On the contrary, this recovery decreases to 48% when only one face is available for imbibition as in the condition of OEO. Since we are dealing with a 2-D model, both TEO and TEC have two faces open to flow and hence they are expected to have almost the same recovery factor. However, the surface area open to flow in TEC case is along the j-direction thus allowing the displacement of oil along the horizontal axis to be more efficient.

The difference in the amount of oil recovered between the AFO and OEO boundary condition is only 4%.; however, the time needed to achieve this maximum recovery varies greatly. This can be seen in **Figure 15** where the time needed to fully recover the oil from the core and reach to the residual oil saturation for OEO boundary

condition is almost 8 times the time when the AFO condition is simulated. This confirms that the number of faces available for imbibition greatly affects the time utilized to almost recover the same amount of oil from the different boundary conditions' cases

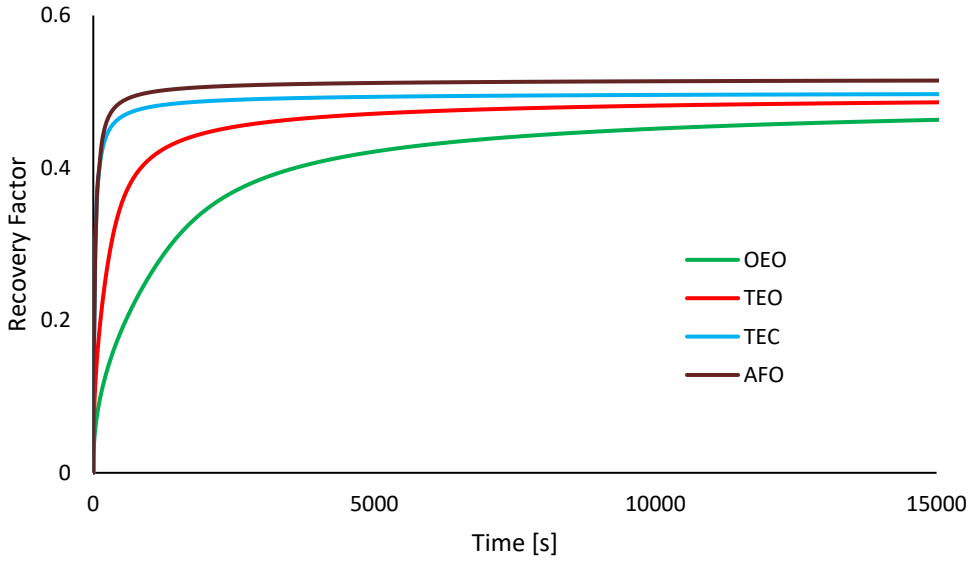

Figure 14 Recovered oil for different boundary conditions produced by means of numerical simulation

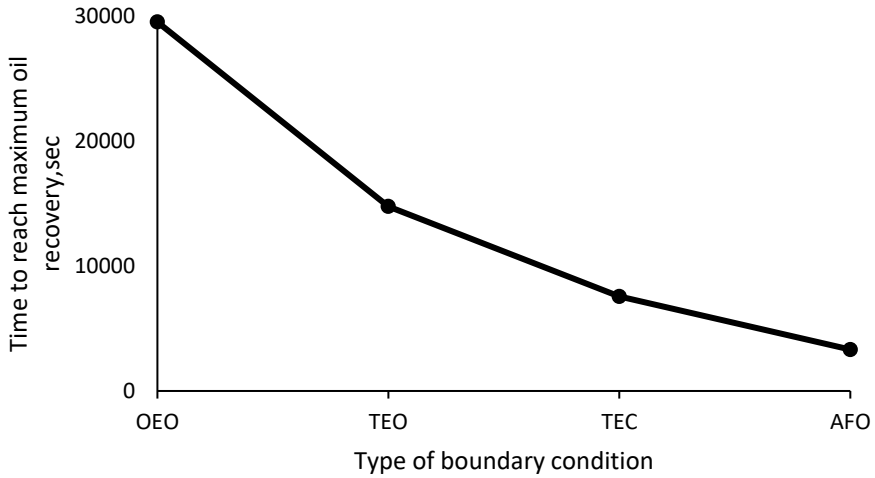

Figure 15 The graph shows the time needed to reach residual oil saturation as a function of the faces exposed to imbibition per boundary condition

5.2 Calibration of the Analytical Model to Simulation Results

Predicting oil recovery from reservoir matrix blocks can be a tedious process. Moreover, the simulators used to calculate oil recovery from field data often face the problem of increased computing time until a satisfactory solution is converged to. However, many researchers claim that scaling the imbibition rate through scaling laws can reduce the simulation time of the process significantly when integrated into field scale simulators (Morrow and Mason, 2001).

The counter-current imbibition results discussed earlier are hence used to evaluate the validity of a new modified so-called 'master' scaling group developed by Schmid et al., (2012) and is independent of rock and fluid type and the wetting condition of the rock. In our study, numerical approaches were used to test the applicability of the scaling equation for the four examined boundary conditions. The analytical results of the oil recovered by the spontaneous imbibition mechanism were plotted against the non-dimensional time of **Eq. 3.9** on a semi-log scale. The plots presented in **Figure 16-a** and **Figure 16-b** revealed the importance of normalizing the core length into different characteristic lengths per case to achieve unity in the curves. The early imbibition time t^* is shown as well to indicate the region $0 < t < t^*$ where the analytical solution is valid.

The volume of oil recovered was calculated based on the assumption that the volume of fluid is conserved in a counter-current spontaneous imbibition case where there is no flow across across the boundaries of the system. Hence, the volume of the cumulative water imbibed into the core sample calculated from the analytical solution should be equal

to the volume of oil recovered from the core and is represented in the following equation from Schmid et al. (2012):

$$Q_w(t) = \int_0^t q_w(0,t)dt = 2Ct^{1/2} \qquad \textbf{(5.1)}$$

The plots in **Figure 15** indicated how the recovery curves at different boundary conditions generated using the analytical solution would fall into almost one curve when the dimensionless time is used.

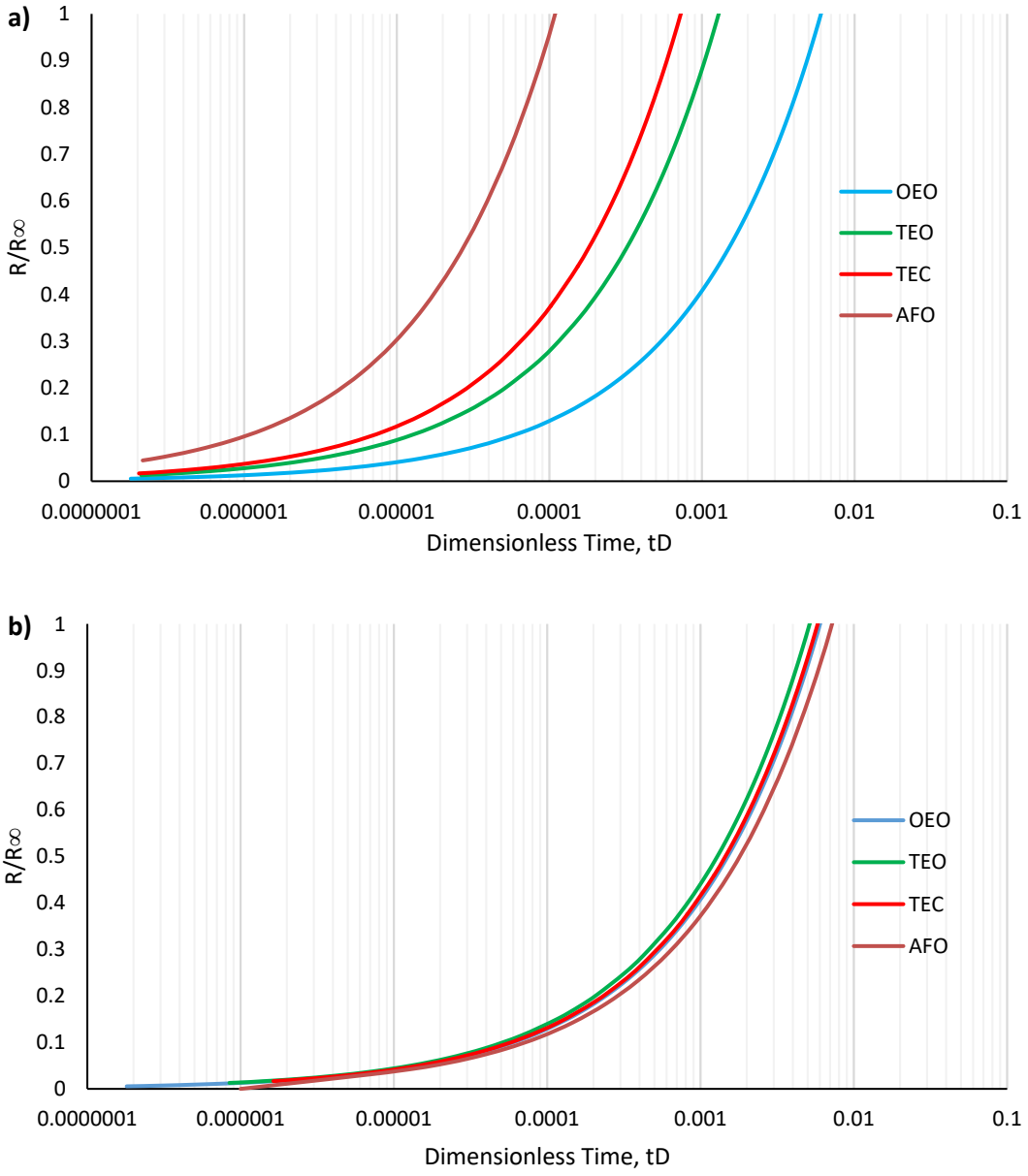

Figure 16 Recovery of the oil displaced versus time. (a) Time is scaled according to the scaling group proposed by Schmid et al. (2012). The data did not collapse into one curve since the characteristic length per case was not used in the equation. (b) In this graph, we used the equation mentioned in table 3 to calculate the characteristic length for the different cases presented in figure 4. We can see that the data falls neatly into almost one single curve indicating that the represented length of the core should be replaced as per the boundary condition requirement.

5.3 Testing the Validity of the Scaling Group

Now, we compare the results of imbibition assisted oil obtained numerically to those calculated with the analytical solution, This will allow us to verify whether there will be a match in the shape of the oil recovery curves at the different boundary conditions. The plots in **Figure 17** show a high agreement between the analytical and the numerical solution for the different boundary conditions listed in this study. The results of the simulation scale up nicely with the dimensionless time proposed thus validating the scale group. Furthermore, scaling the simulation data and the average analytical solution of the four cases with the dimensionless time (t_D) show that both solutions fall into a neat curve. Regardless of the boundary condition imposed on the system, only a little scatter is observed around the analytical solution. Notice that the solution is only valid as the condition $t_D < t^*$ is satisfied

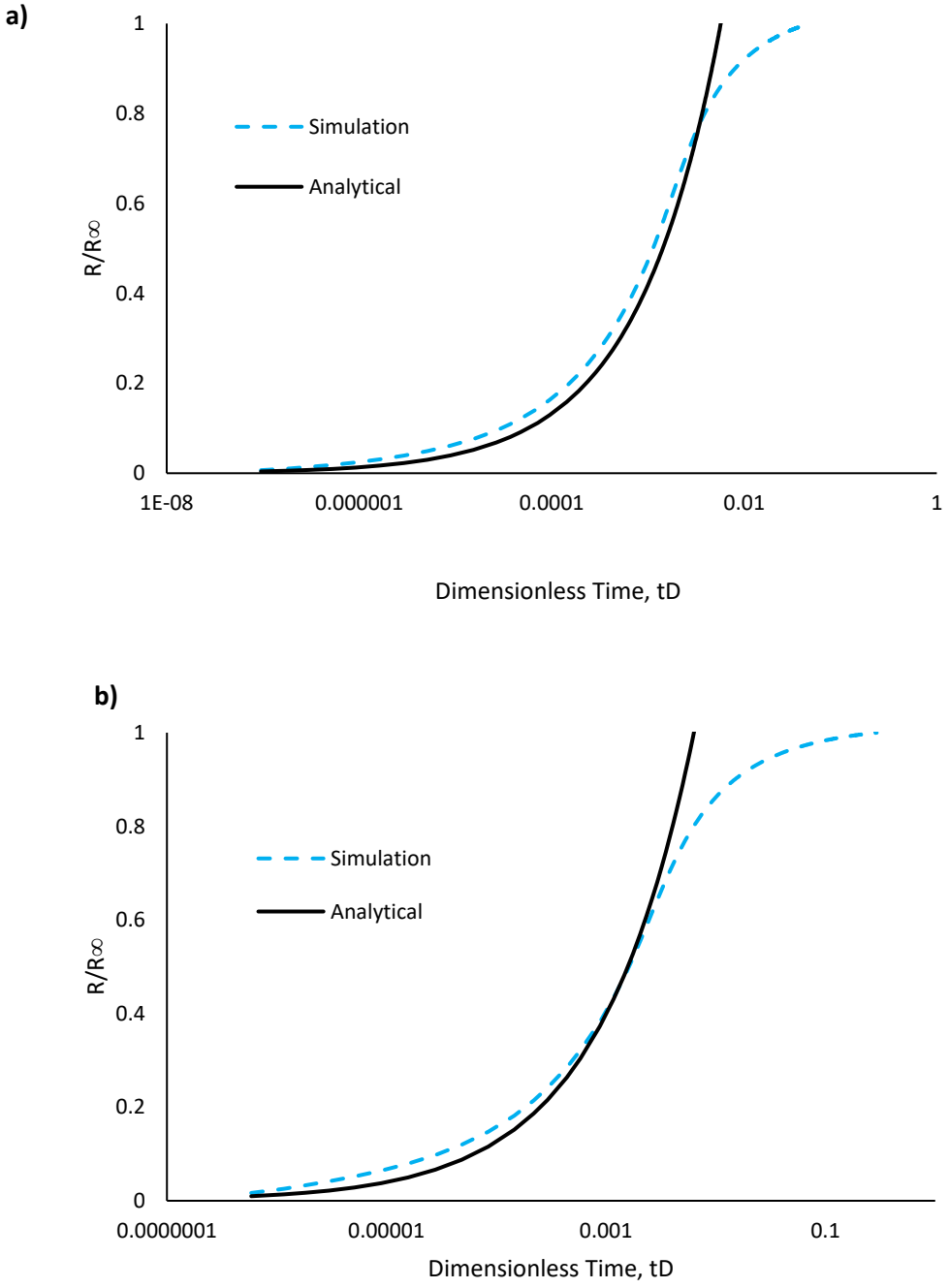

Figure 17 Recovery of the oil displaced versus time. The analytical solution is compared with the numerical results for the different boundary conditions presented in table 3. The simulation in general shows a high agreement with the analytical solution upon using the scaling group. The cases are labeled as a, b, c and d to represent OEO, TEC, TEO and AFO respectively.

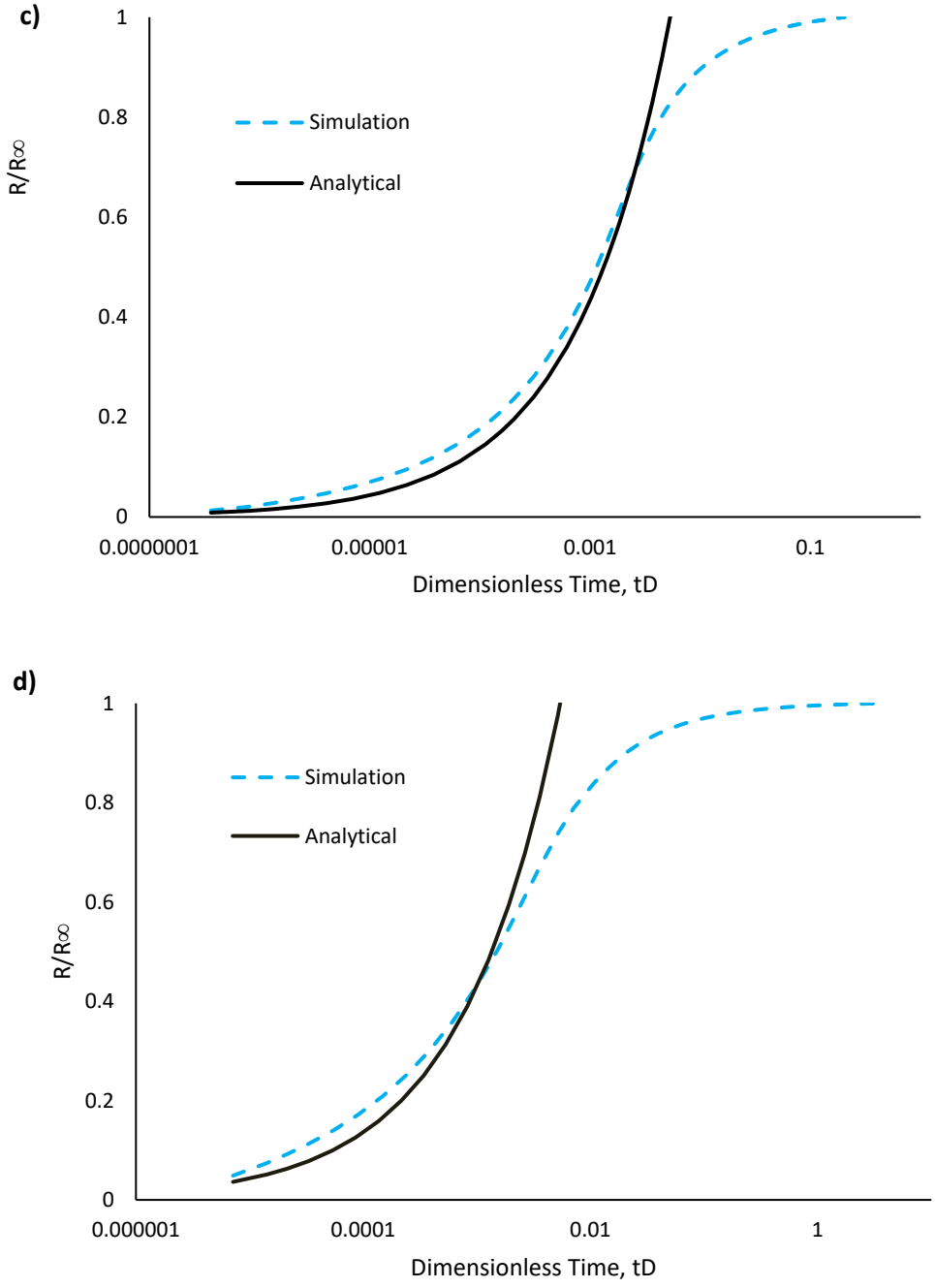

Figure 17 Continued

However, observing the AFO case closely, we see that the match between the two data sets is not perfect. This is due to the complexity of the simulated case where the core is exposed to flow from four different faces. One reason for such discrepancies can be attributed to the grid size used in the simulation. The 50×50×1 might not be able to capture the changes in the saturation profile as the flow is coming from four different faces in 2-D. For this purpose, we simulated the AFO case again with 100×100×1 grid size model that will allow us to achieve higher accuracy in predicting recovery behavior. Furthermore, we applied refined gridding technique to the 100×100×1 model to create a tartan grid that allows the monitoring of the changes in the saturation profile at early time. As we approach the center of the core at late imbibition times, a coarser grid is used since the results from that section is irrelevant to the analytical solution. The discretization of the model into different grids with different dimensions is called Local grid refinement (LGR). The new resultant grid is displayed in **Figure 18.**

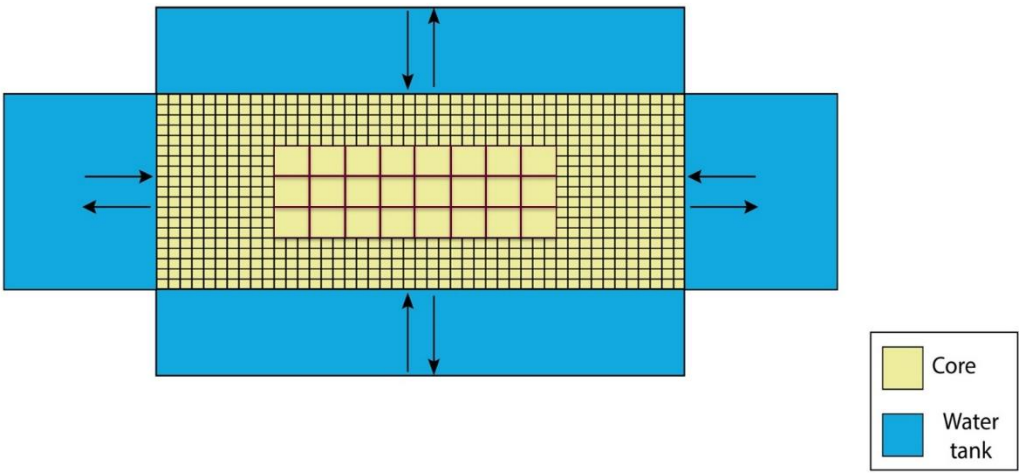

Figure 18 The illustration shows a 2-D grid with AFO boundary conditions. The center of the grid is coarse compared to the grids close to the boundary.

The results plotted in **Figure 19** shows that the analytical solution along with the different recovery profiles for the AFO case. We can clearly notice that the degree of correlation increased with finer grid size when 100×100×1 model is used. Furthermore, the utilization of the refined gridding technique achieved an even closer fit to the analytical solution up to the early imbibition time *t** at 0.01. In general, it is worth saying that AFO case involve complex flow movements and the simulation might fall short in predicting the recovery accurately from such a process.

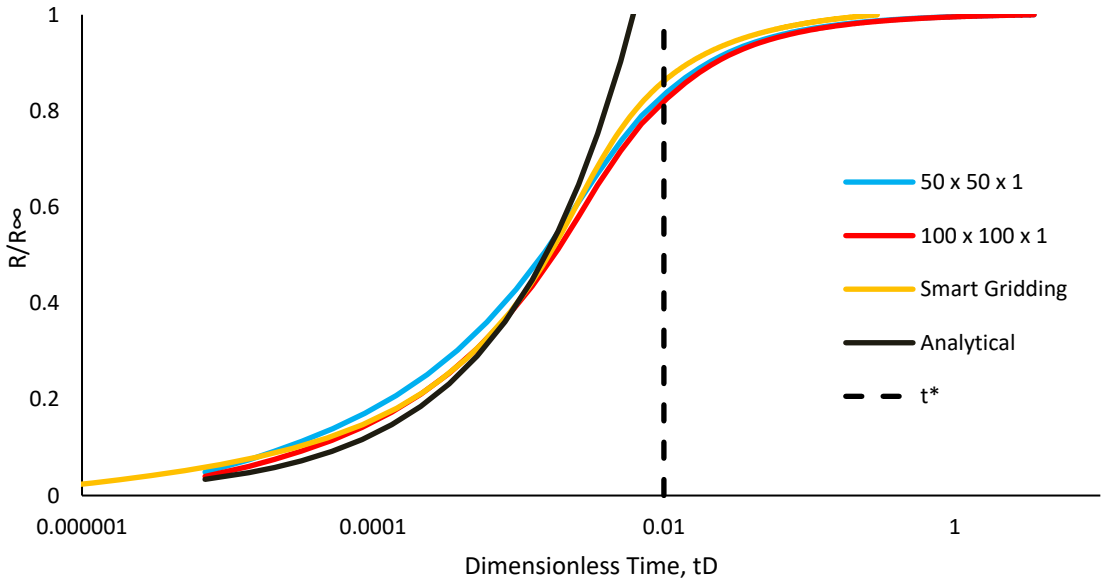

Figure 19 The plot shows the ultimate recovery of oil as function of the dimensionless time. The finer grid size shows clearly a better fit with the analytical solution compared to the 50x50x1 model. The fit gets even better when even finer grids are used to the areas close to the boundaries and thus allows the capturing of final saturation changes. The smart gridding technique shows the best fit with the analytical solution but it is only valid till the early imbibition time, t*.

Examining the results further, we noticed that regardless of the faces available for imbibition, the oil recovery scaled smoothly with the dimensionless groups and fell neatly into a narrow range of data (**Figure 20**). Therefore, the results of the spontaneous imbibition obtained through simulation correlate greatly with that derived from the analytical solution proposed by the new master dimensionless scaling group. The data are reduced to single curve in spite of the fact that the characteristic length varies greatly from one case and the other (0.81 cm < *Lc* < 7.66 cm)

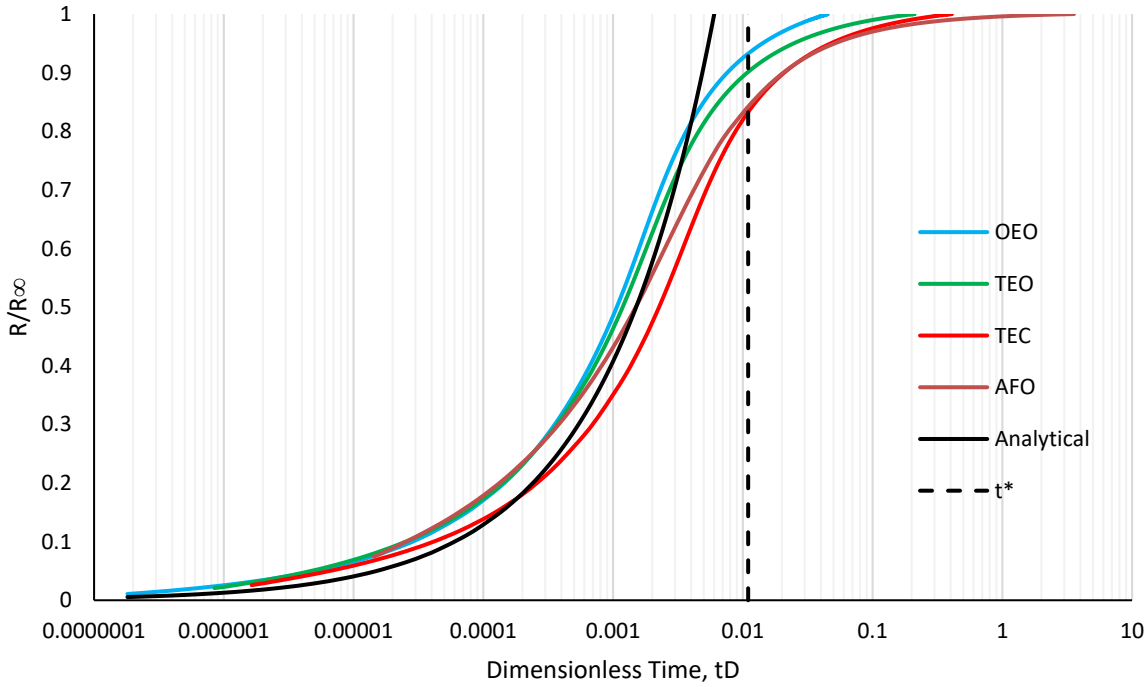

Figure 20 The plot shows normalized oil recovery factor is plotted against time. Time is scaled according to Schmid et al (2012) model resulting in the data to collapse into one curve on a semi-log scale. The scatter of the data is reasonable and within the range

CHAPTER VI

PARAMETRIC STUDY OF THE SCALING IMBIBITION OF SPONTANEOUS IMBIBITION

In this Chapter, we will investigate the effects of the variations in water-oil viscosity ratio, sample shape, wettability, relative permeability and initial water saturation on the validation of the Schmid and Geiger (2012) scaling group. The main purpose is to vary each parameter independently to identify the trends in imbibition behavior. The results will be compared with the analytical solution to confirm if it succeeds in predicting the scaling of the data regardless on the range of parameters used.

6.1 Choosing a Simulation Model

Assuming a counter-current spontaneous imbibition with TEO, the volume of water imbibed against time is plotted in **Figure 21** for the base case and represents the volume of oil that can be produced from the simulated core. It is observed that the analytical solution and the 2D numerical simulations match closely for early time imbibition region when $t < t^*$ and $t^* = 210$ seconds. Moreover, the normalized recovery was plotted against the dimensionless time of Schmid and Geiger (2012) in **Figure 22** proves that this technique may be suitable for scaling up lab results to field-scale recovery.

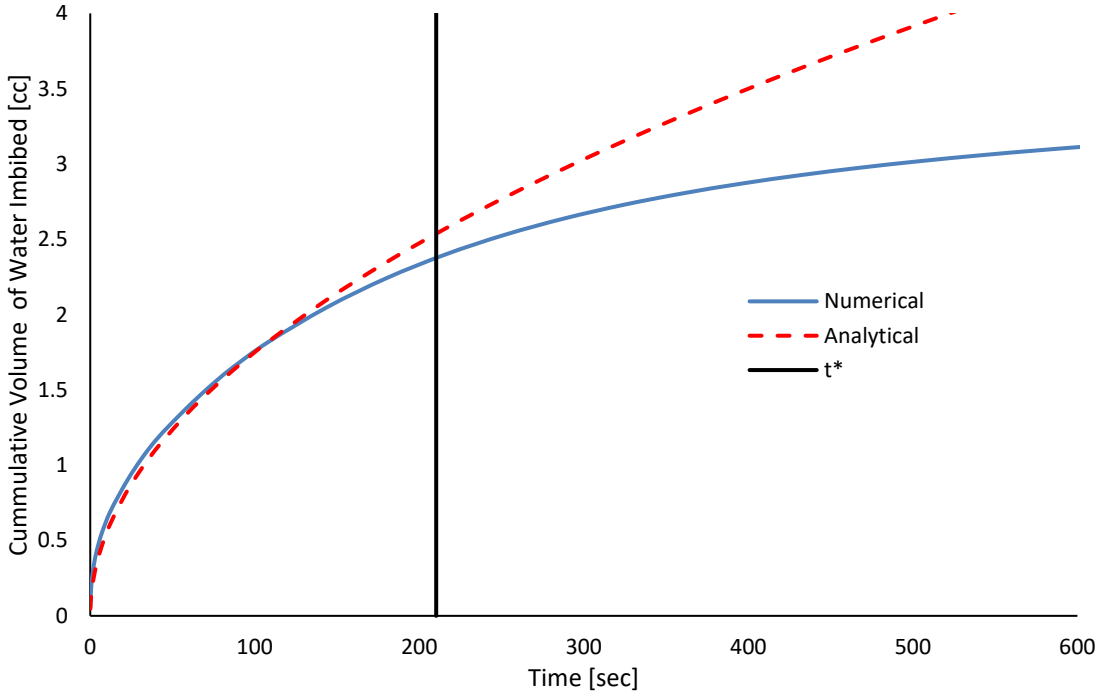

Figure 21 Graph of cumulative volume of water imbibed against time shows that the analytical and numerical models match for the early imbibition time before *t**with a slight margin of error.

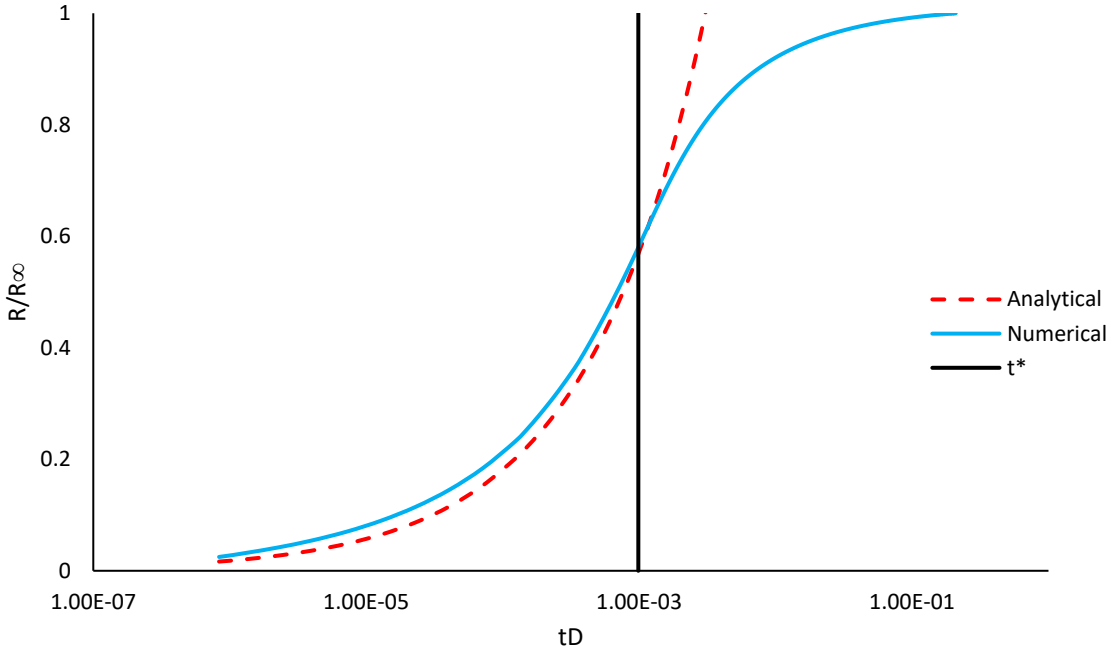

Figure 22 Graphs of normalized recovery against dimensionless time, *tD*. The analytical and numerical solutions exhibit a good match with as light margin of error.

6.2 Effect of Capillary Pressure

The capillary pressure curves, as stated earlier, are generated based on **Eq. 4.3** The exponent *l* controls the shape of the curve as all the other parameters are fixed for the same case. The values of *l* were varied to examine the effect on the simulation results and **Table 5** summarizes the values of *l* used and the corresponding *C* value for each case. The *Pc* curves for the different cases are plotted in **Figure 23.**

Table 5 The parameter *l* and the corresponding *C* values.

l	***C [m/√s]***
-0.2	2.5×10^{-5}
-0.5	3.7×10^{-5}
-0.7 (base case)	5.3×10^{-5}
-1	6.1×10^{-5}
-2	1.10×10^{-4}

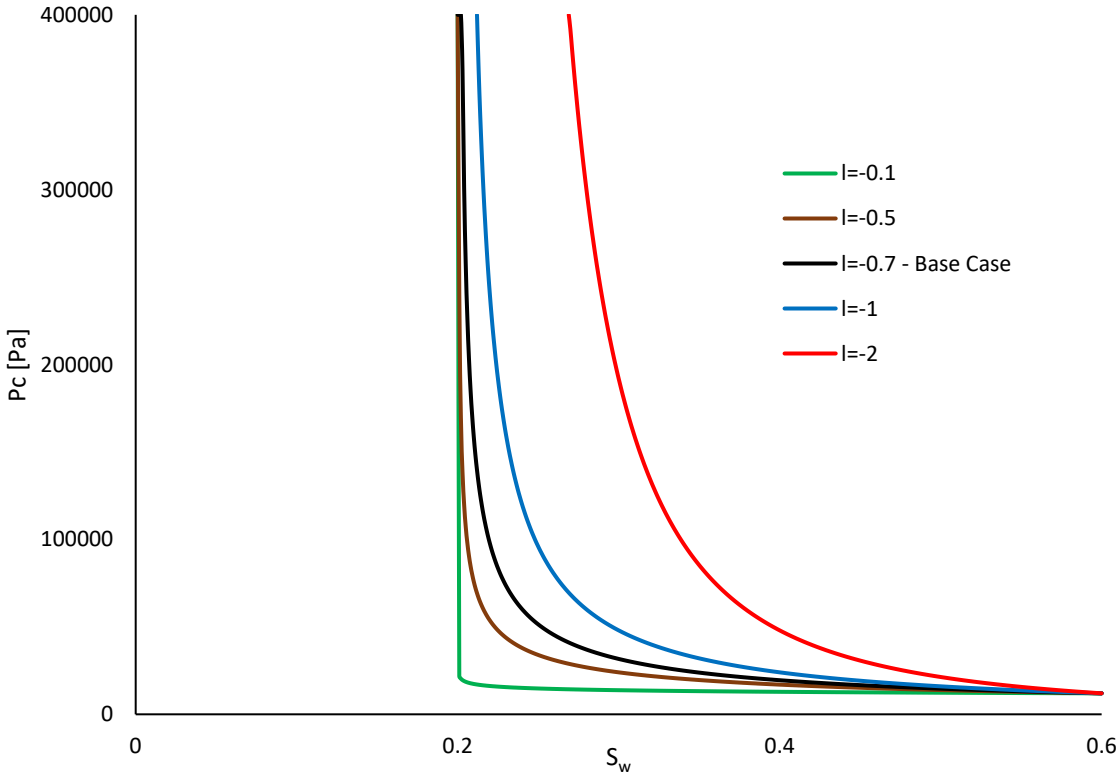

Figure 23 Capillary pressure curves plotted against water saturation for different l values

The shape of the capillary pressure curve affects directly the recovery of oil. The recovery is faster when the change in the *Pc* values is bigger. Technically, the capillary difference is what drives the flow of the oil in the reservoir. The normalized recovery is plotted against time on a semi-log scale in **Figure 24-a** where the change in time is in 100 orders of magnitude. However, when a similar plot in **Figure 24-b** is generated through the dimensionless time of the suggested scaling group, the difference between the difference cases in *tD* values is less than one order of magnitude. Furthermore, the average analytical solution is determined for the various aforementioned cases and graphed in **Figure 24-b** showing a close match that allows the analytical solution to predict the performance of the numerical simulators regardless of the shape of the capillary curve.

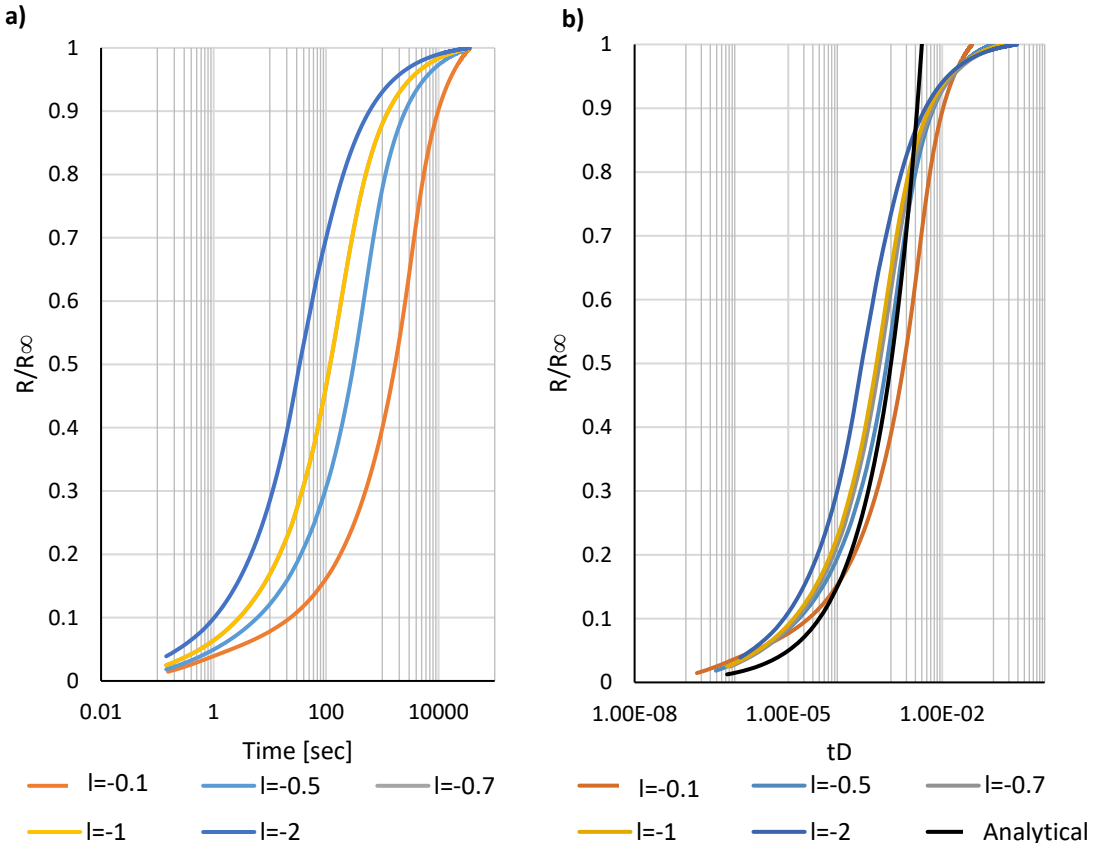

Figure 24 Normalized recovery is plotted against normal time (a) and dimensionless time (b). It is clear that the scaling group reduces the scatter in the data significantly and the analytical solution in (b) matches with the coinciding simulated data.

6.3 Effect of Relative Permeability

6.3.1 Shape of Oil Curve

The exponent *m* in Corey relation determines the shape of the relative permeability curve to oil. The plot in **Figure 25** shows the different profiles when *m* is varied, and **Table 6** summarizes the *m* and *C* values for each case. It is evident that when *m* is equal to one, the oil curve is linear thus representing the limiting value of the exponent.

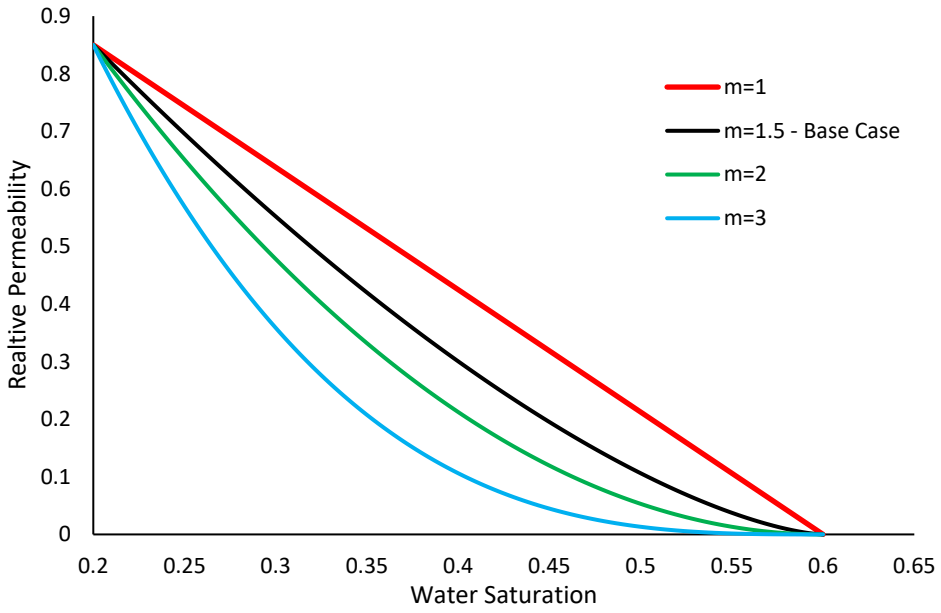

Figure 25 Relative permeability of water plotted against water saturation for different m values.

Table 6 The variation in parameter m and the corresponding C values.

m	***C [m/√s]***
1	5.3×10^{-5}
1.5 (base case)	4.6×10^{-5}
2	4.09×10^{-5}
3	3.3×10^{-5}

The **Figure 26-a and 26-b** represents normalized oil recovery plotted against time and dimensionless time respectively. We do not see significant variations between the oil recovery profiles on the normal scale of time. Moreover, the dimensionless time brings the profiles even closer and it can be see that they are almost coinciding. The analytical solution in **Figure 26-b** is not a close fit to the numerical simulation however it is still considerably a good match for the simulated results. The results showed a high agreement with the scaling group regardless of the *m* values thus proving its validity. Nevertheless, at high values of *tD*, the results scatter around the base case and is attributed to low permeabilities of oil with increasing saturation. Usually, k_{ro} has low on SI upscaling and this was evident from this analaysis.

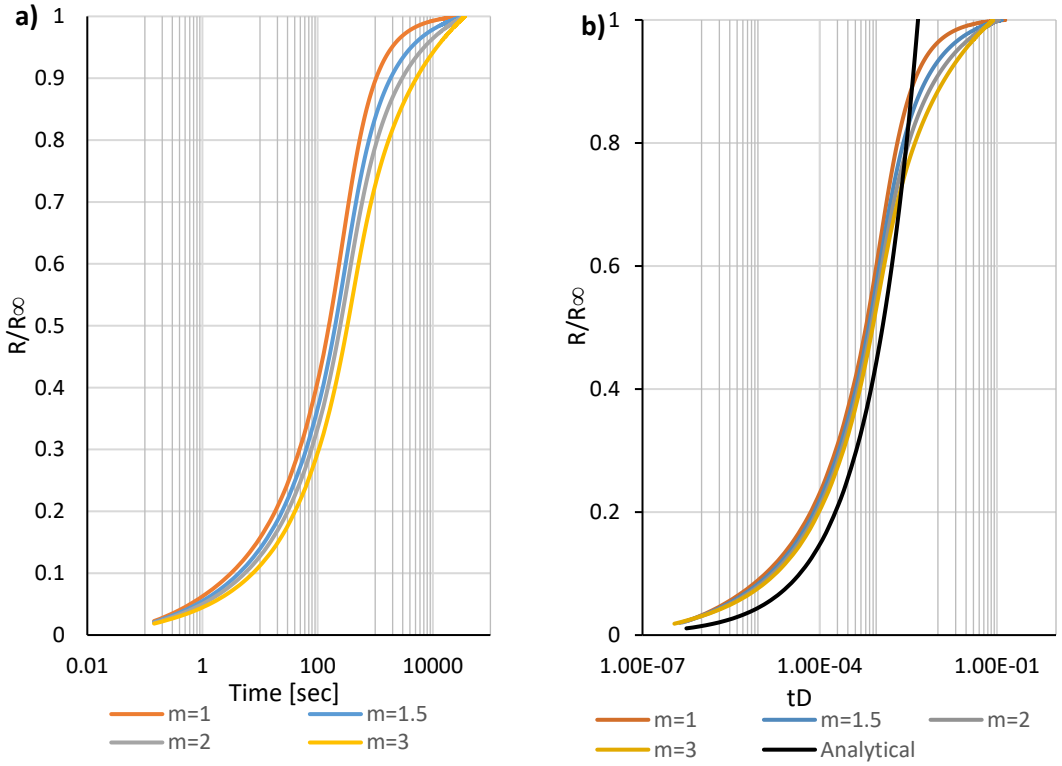

Figure 26 Normalized recovery is plotted against normal time (a) and dimensionless time (b). The effect of the scaling group is minimal on the simulation results and the analytical solution in (b) matches roughly the plotted data sets.

6.3.2 Shape of Water Curve

The exponent *n* is varied similarly to the previously discussed case and **Table 7** summarizes the different n values along with the *C* values for each case. The curves of the water relative permeability as a function of water saturation is shown in **Figure 27**. The oil recovery results of the simulation show a close match between the cases when plotted on a logarithmic scale of time in **Figure 28**. Small differences are observed but are less than an order of magnitude. However, when the scaling group is used, these small variations disappears an almost replication of the fractional recovery graph is observed for the different cases. Moreover, the average analytical solution matches perfectly with the

numerical solutions. Even for extreme values of n leading to significant changes in the shape of the water phase relative permeabilities, the scaling group proves that it is independent of this parameter.

Table 7 The variation in parameter n and the corresponding C values.

n	***C [m/√s]***
1	9.50×10^{-5}
2	6.18×10^{-5}
3 (base case)	4.70×10^{-5}
4	3.73×10^{-5}

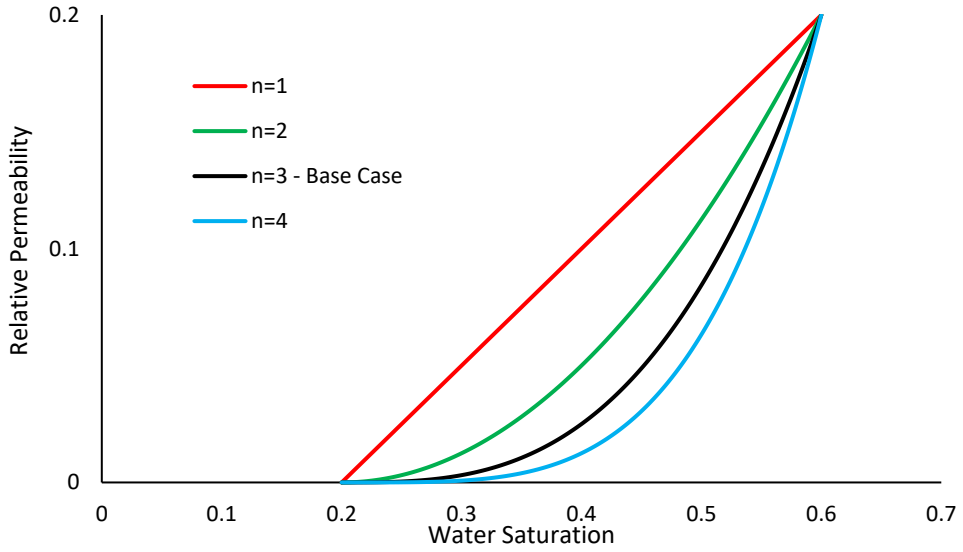

Figure 27 Relative permeability of oil plotted against water saturation for different n values

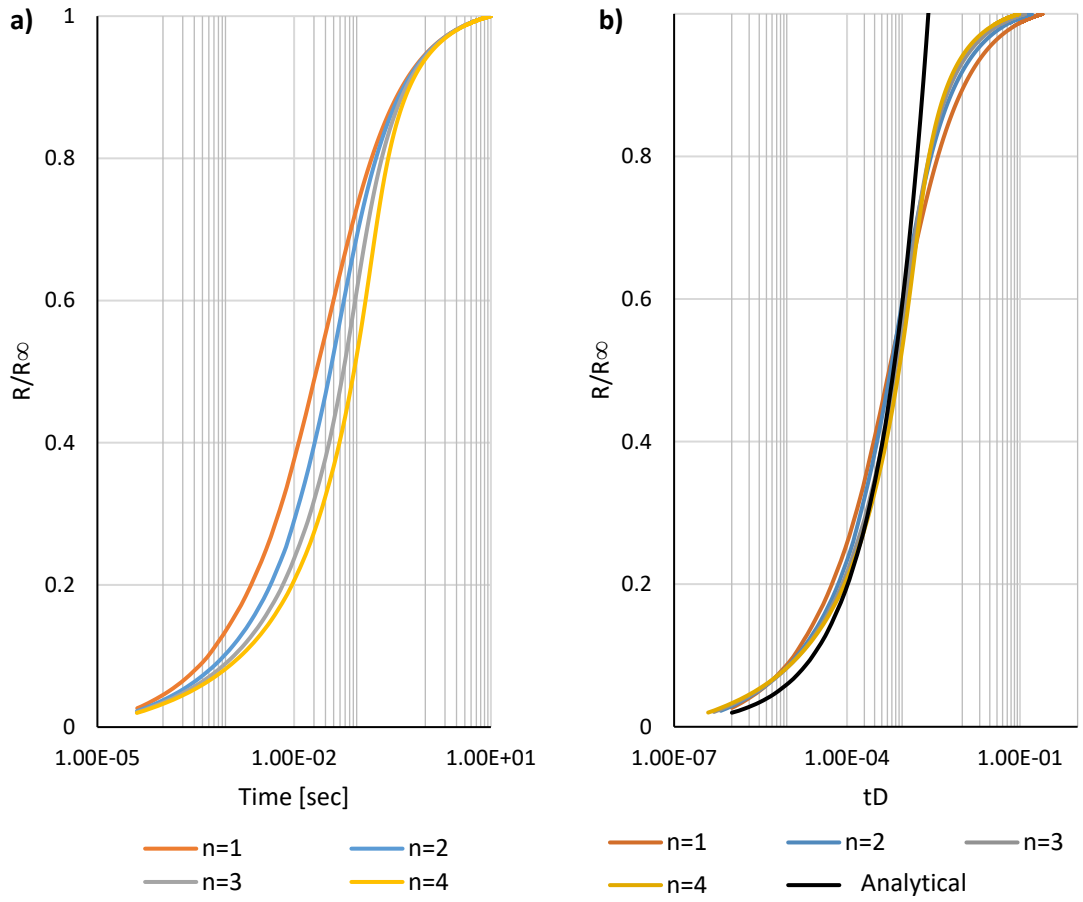

Figure 28 Normalized recovery is plotted against normal time (a) and dimensionless time (b). The scaling group efficiently groups the simulated data regardless of the variation of exponent of oil relative permeability. The analytical solution fits perfectly the simulated data plotted in (b)

6.3.3 Shape of Water Curve

Table 8 summarizes the different values of the water end-point relative permeability, $k_{rw,max}$ and the *C* value for each case. This information is used to plot the different cases as a function of water saturation in **Figure 29**. The simulated curves when plotted with time show faster recovery for higher $k_{rw,max}$ values. The observed curves do not scale with time which is an expected result. However, when the dimensionless time is used in **Figure 30**, the curves scale up nicely and scatter around the average analytical

solution thus validating the scaling group. An exception to the matched curves is the case of $k_{rw,max}$=0.02 and could be explained by the slow movement of water due to low relative permeability values.

Table 8 The variation in parameter n and the corresponding C values.

$k_{rw,max}$	$C\ [m/\sqrt{s}]$
0.3	0.000052
0.2 (base case)	0.000047
0.1	3.70E-05
0.05	2.9E-05
0.02	2.1E-05

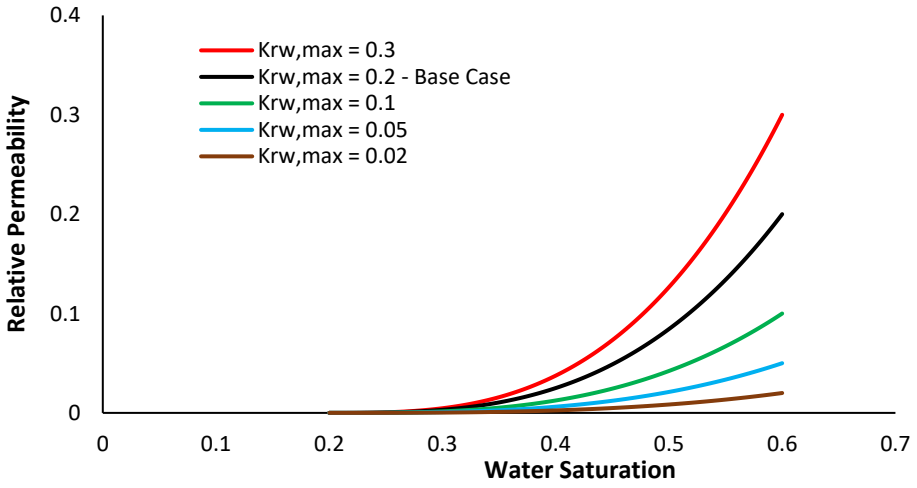

Figure 29 Water relative permeability curves plotted against water saturation for different krw values.

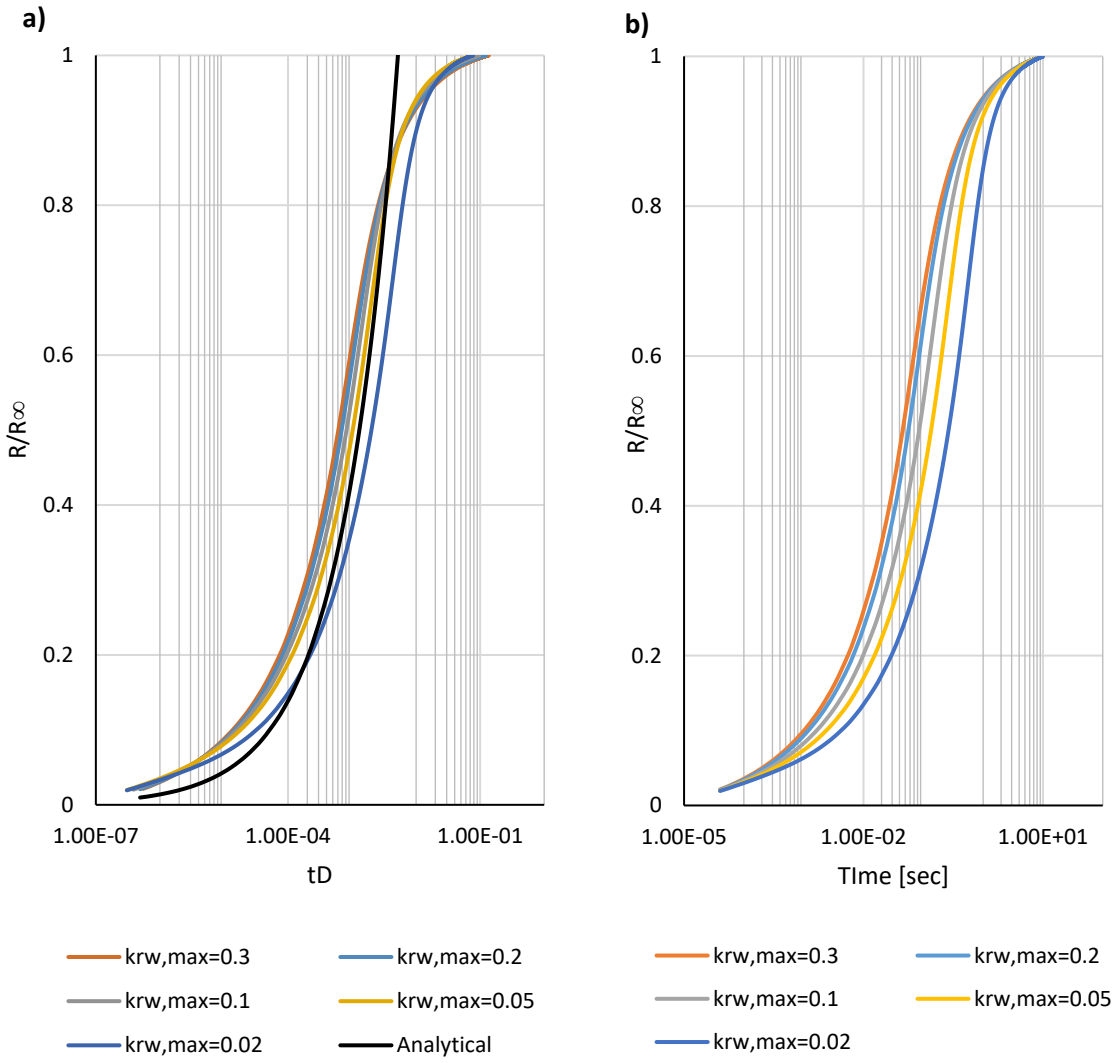

Figure 30 Normalized recovery is plotted against dimensionless time (a) and normal time (b). The data spread over 5 orders of magnitude when normal time is used. However, the variations decrease considerably and match with the numerical solution when plotted against dimensionless time.

6.4 Effect of Initial Water Saturation

The effect of initial water saturation on oil recovery by imbibition has been long studied by scientists (Akin and Kovscek, 1999; Cil et al., 1998; Viksund et al., 1998; Du Prey, 1978; Mason and Morrow, 2001). It has been noticed that imbibition rate and final recovery both decrease with an increase in initial water saturation for imbibition assisted oil recovery (Zhou et al., 2000). The recovery curves plotted in **Figure 31** proves this conclusion as the oil recovery increases for decreasing initial water saturation which was varied between 0 and 0.4. This result also proves the efficiency of our simulation code as it systematically predicted the oil recoveries without any noticeable errors. The summary of the different cases with the correspsong *C* value are presented in **Table 9**.

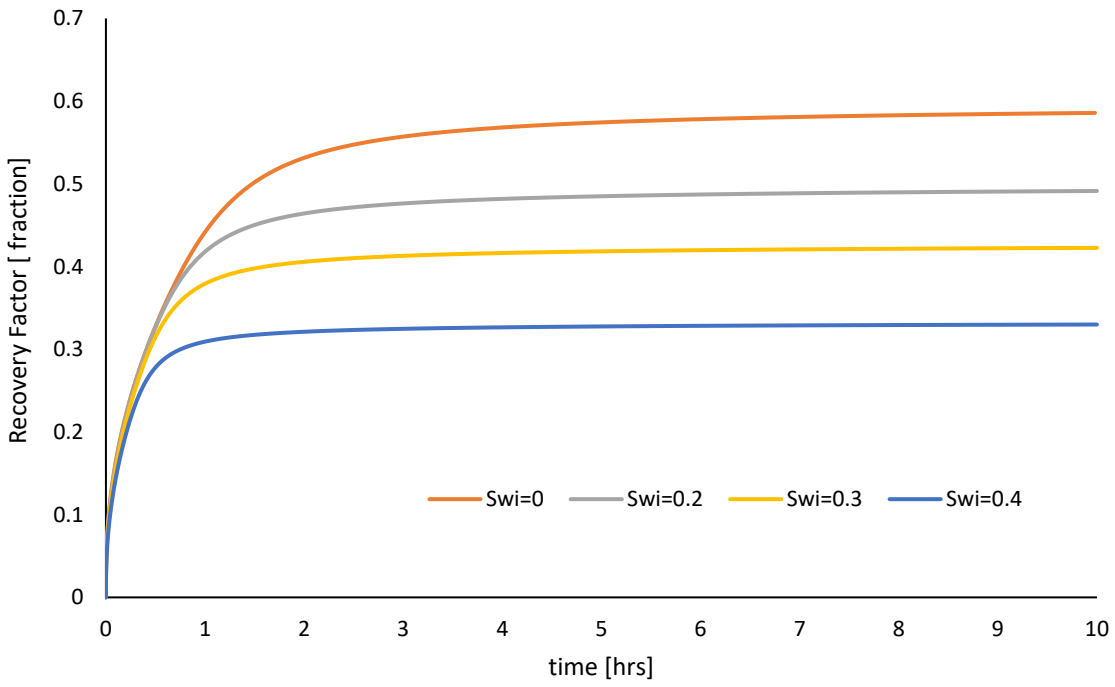

Figure 31 The plot shows the recovery factor for different initial water saturation values changing with time.

Table 9 The table shows different C values for varying S_{wi}

Swi	***C [m/√s]***
0	2.52×10^{-5}
0.2 (base case)	2.06×10^{-5}
0.3	1.7×10^{-5}
0.4	1.46×10^{-5}

The effect of initial of water saturation on oil recovery affects directly the recovery factor of oil. As the connate water saturation decreases, more oil is stored in the pores and thus flushed out by the means of spontaneous imbibition. This process of displacement is not affected by the initial water saturation of the rock as the flow properties are sustained for different S_{wi} values. Hence, it is expected to have similar curves for ultimate recovery when the oil recovery data is normalized and plotted with time and dimensionless time. If we look closely at **Figure 32-a** and **32-b**, we can see that the recovery curves are almost matching, and the scaling group did not have any effect on the simulated data.

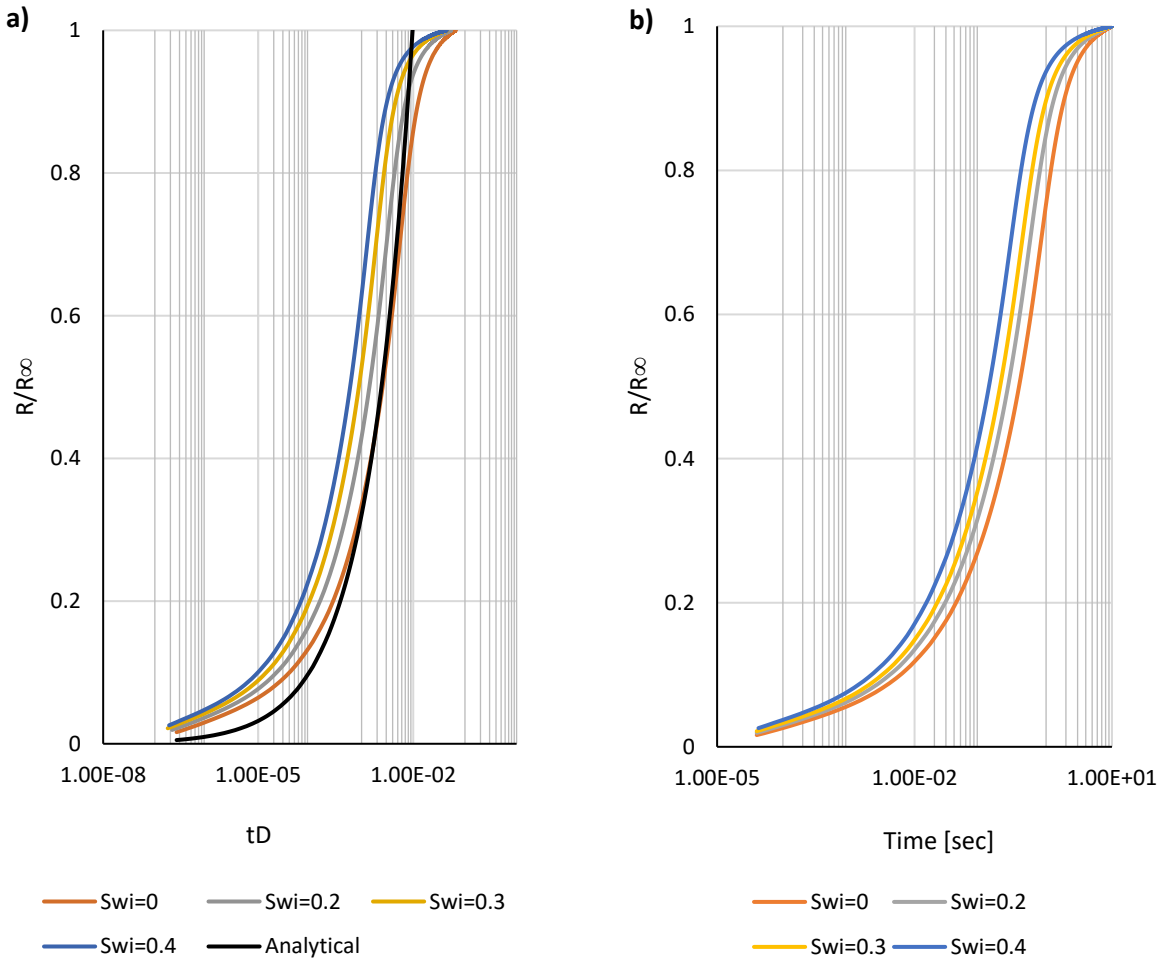

Figure 32 The ultimate normalized recovery is plotted against dimensionless time (a) and normal time (b). The data is spread over the same range of time regardless whether normal time or the scaling group is used. The scaling group did not have any effect on brining the data closer together.

6.5 Effect of Viscosity Ratio

We define viscosity ratio is defined as the ratio of the viscosity of the wetting phase to that of the non-wetting phase and is denoted by M. In our case, water is the wetting phase while oil is the non-wetting phase. The viscosity values used in the base case of the simulations are 1 cP and 3 cP for water and oil respectively. We simulated two cases with different viscosity ratios 1 and 0.1 and compared them with the recovery oil curves obtained from the base case simulation. The graphs in **Figure 33-**a and **33-b** showed evidently that the recovery curves scale up with the dimensionless time opposed to the normal time in **Figure 33-a**. Small differences are noticed at late times and can be attribute to the effect of boundary of the porous media on the SI process. The average analytical solution is plotted in **Figure 33-b** and matches nicely with the simulated data. The curves also show that recovery is faster and more efficient with lower oil viscosity.

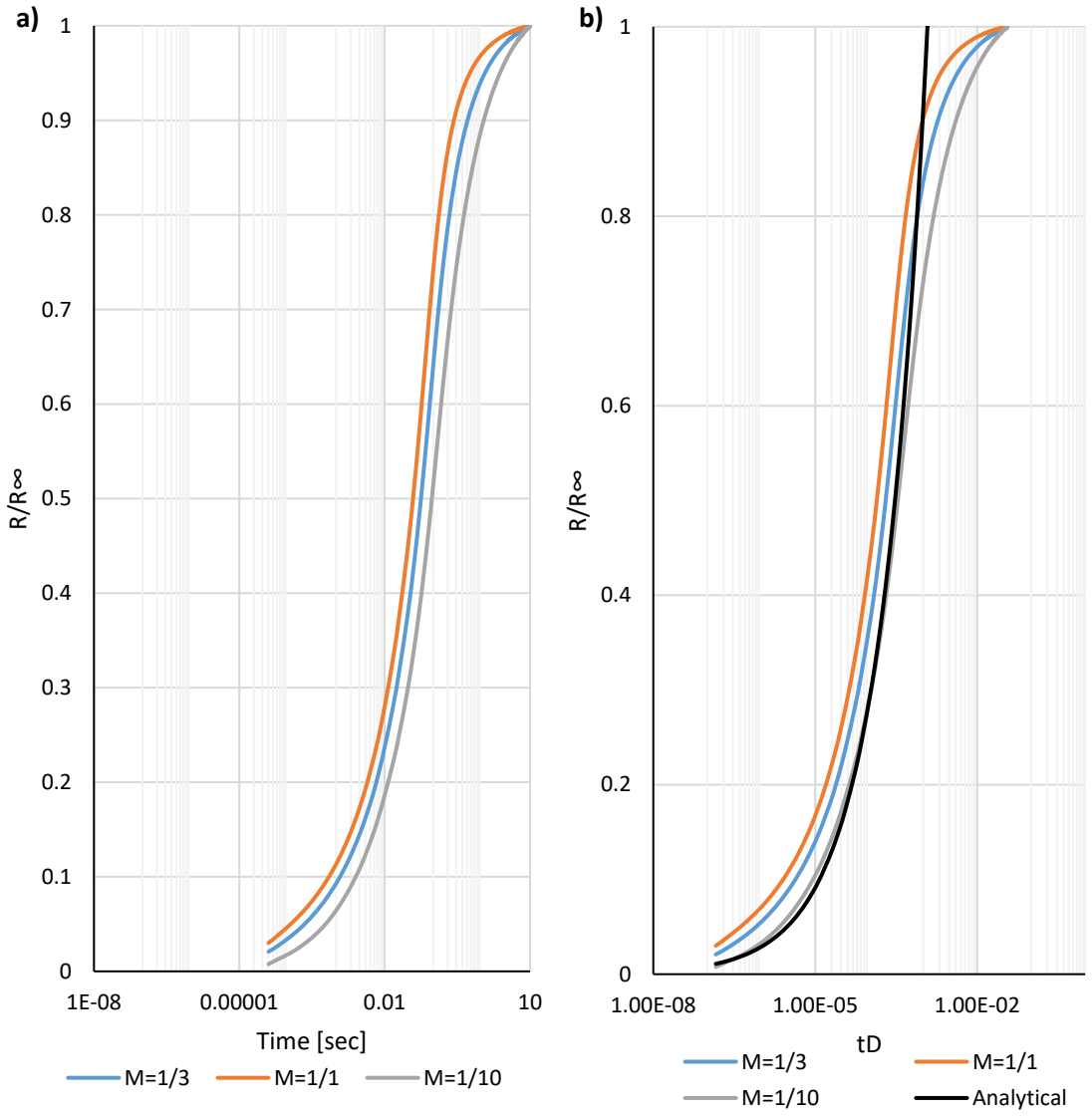

Figure 33 The plot in (a) shows the normalized recovery with normal time while dimensionless time is used for scaling in (b). The range of recovery data in (b) is tighter than the range in (a) for the same viscosity ratios. The data scaled up with dimensionless time and matched the analytical solution smoothly.

6.6 Effect of Wettability

In this section, we will study the effect of wettability on the upscaling of both co-current and counter current spontaneous imbibition. The wettability study is performed on a 1-D homogenous porous model consisting of 400 grids in the x-direction. The counter-current imbibition is represented by OEO boundary condition with zero capillary pressure at the open boundary. On the contrary, the co-current model has two wells at the extreme ends of the core with one acting as producer and the other injecting water in the water tank as observed in **Figure 34**. The rate of production and injection is controlled by the bottom-hole pressure of the two wells to ensure the pressure is balanced throughout the system with maximum oil recovery achieved. The input parameters used to generate the various cases in **Table 10** were based on Schmid et al., 2016 study.

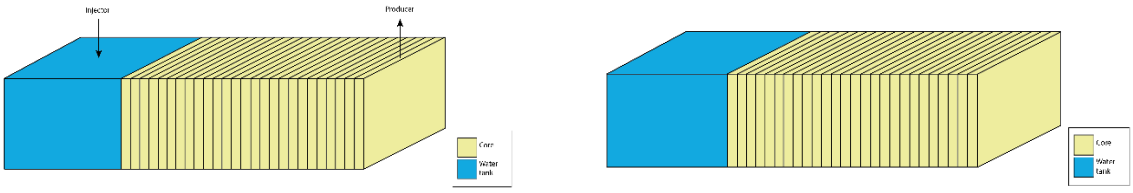

Figure 34 The illustration on the left (a) shows grid model for co-current spontaneous imbibition, while the illustration on the right (b) shows grid model for counter-current spontaneous imbibition of an oil-water system.

Table 10 This table shows the parameters used to solve for the analytical solution and the obtained C values for co-current and counter-current SI with varying wetting cases.

Parameter	Strongly Water Wet (SWW)	Weakly Water Wet (WWW)	Mixed Wet (MW)
S_{wi}	0.2	0.2	0.2
S_{or}	0.4	0.2	0.1
$k_{rw\ max}$	0.2	0.5	0.6
n	3	3	3
$k_{ro\ max}$	0.85	0.8	0.8
m	1.5	5	8
$P_{entry}\ [Pa]$	12000	12000	12000
I	-0.7	-0.3	-0.2
$[cP]\mu_w$	1	1	1
$[cP]\mu_o$	3	1	1
$C_{co\text{-}current}\ [m/\sqrt{s}]$	9.1308×10^{-5}	2.5×10^{-4}	2.76×10^{-5}
$C_{counter\text{-}current}\ [m/\sqrt{s}]$	4.63×10^{-5}	1.968×10^{-4}	2.75×10^{-5}

The recovery plots in **Figure 35** shows that imbibition assisted oil recovery is minimal for mixed wet rocks. The low water permeability and capillary values could explain this behavior. On the contrary, the strong wet case showed high recovery as expected from the *C* values obtained in **Table 10**. The *C* characterizes the ability of the rock to imbibe water and hence increasing the oil recovered dramatically.

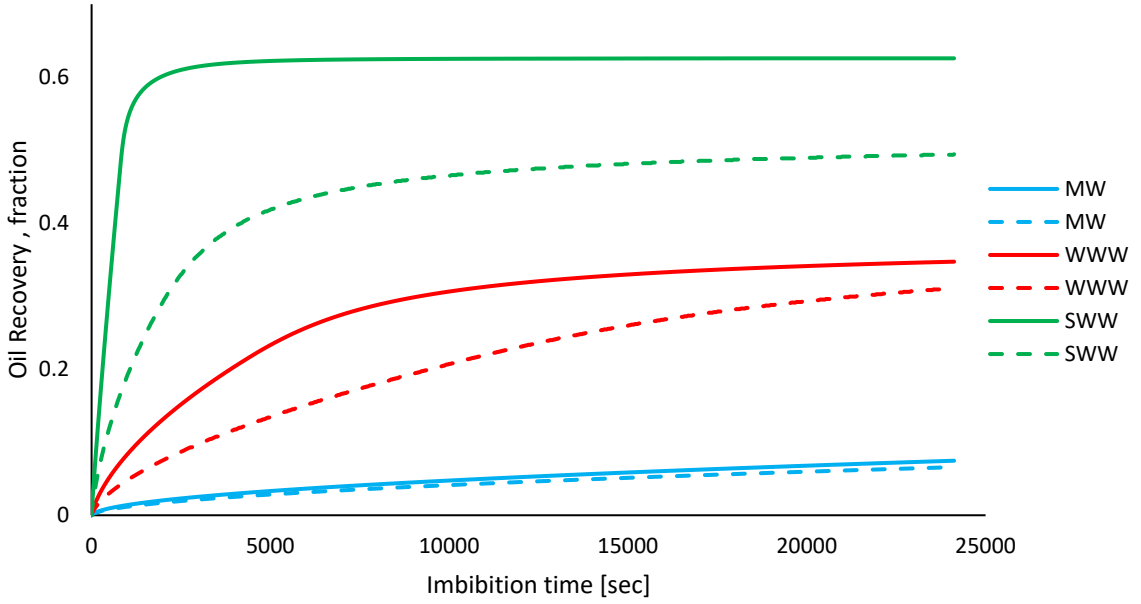

Figure 35 The recovery plots show the amount of oil recovered with time for co-current(solid) and counter-current (dashed) SI with varying wettability of the studied sample. The co-current SI is more efficient regardless of the wetting state and proves superior in recovering more oil. As the wettability of the rock changes from strong wet to mixed wet, the recovery decreases as well following the same trend.

We now compare the scaling of imbibition assisted oil recovery for both co-current and counter-current flow with the analytical solution of Schmid et al. 2011. **Figure 36-a, 36-b and 36-c** show the analytical and the numerical solution for strongly water wet, weakly wet wet and mixed wet cases accordingly. The three plots show a high level of agreement between the counter-current and co-current solutions with the dimensionless time. The average analytical solution can be used to efficiently represent any of the two flow modes with an acceptable margin of error. The level of correlation is the highest for the mixed wet case in **Figure 36-c** as the three curves almost overlap while it is less accurate of the strong wet case in **Figure 36-a**. The co-current flow is much faster in strong wet rocks as the graph suggest and this confirms with the *C* values obtained from the

analytical solution; The *C* in co-current flow is almost double the value of that in the counter-current.

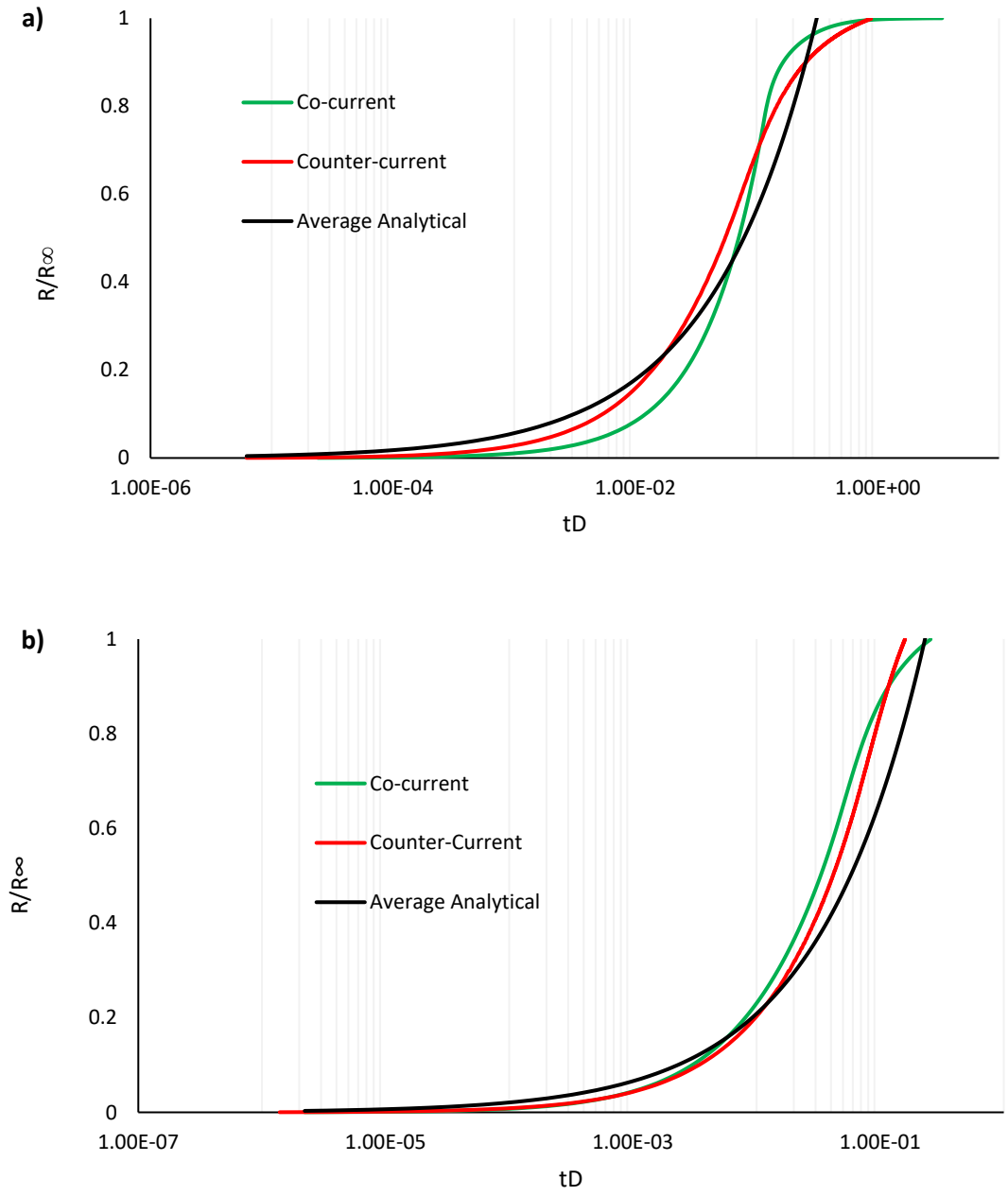

Figure 36 The normalized recovery is scaled with dimensionless time for different wettability cases: strong-wet (a), weak-wet (b) and mixed-wet(c).

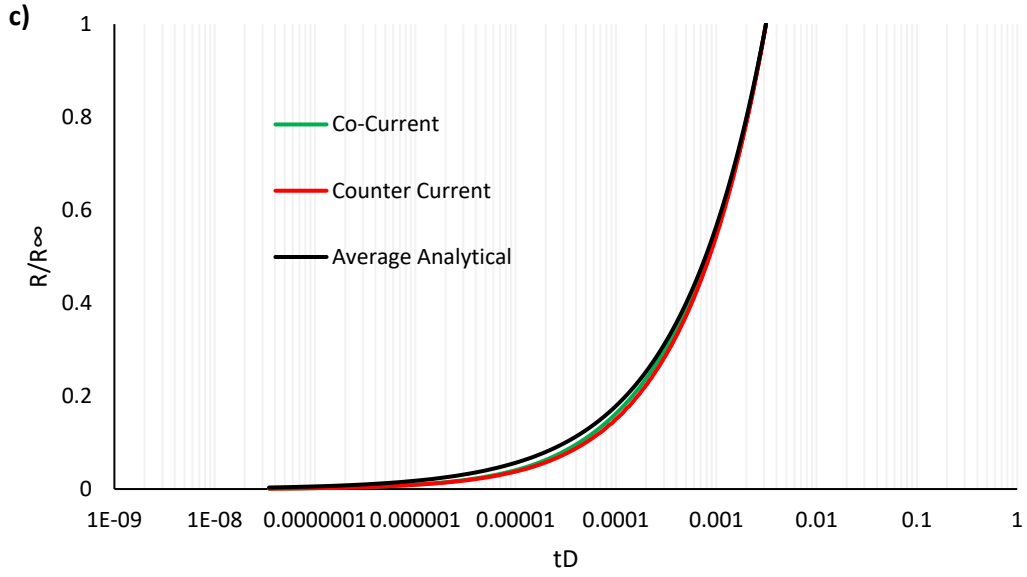

Figure 36 continued

6.7 Effect of Dimensions

In this work, the scope of the numerical investigation was performed through a 2-D grid model. However, the dimensions of the grid play a big role in the convergence of the simulator and thus affects the quality of the results; the finer the grids, the more accurate the results are but more time consuming the process is.

The base model was created using a 50×50×1 Cartesian grid. The model was varied into a 1-D grid of 50×1×1 blocks and a 3-D grid of 50×50×50 blocks using a TEO boundary condition. It was noticed when running the models that the time exhausted by the simulator to run the 3-D model took around 760 seconds, almost 5 times slower than the 2-D model. The 1-D model, on the other hand, took a glance to run with a CPU time of 5.4 seconds. This validates our assumption that finer grids require more simulation time to converge. But the fundamental question is that if this finer model will produce better results when compared to the base model. Although time is of the essence in simulations,

one can sacrifice extra processing time if the quality of the output is unique and accurate. For this purpose, we plotted the oil recovery versus time for the different grid sizes used **(Figure 37)**. The results were expected as the 1-D model showed high discrepancies when compared with the 2-D and 3-D cases. On the contrary, oil recovered using the latter model showed a close correlation between the data sets as the MSE between the 2-D and the 3-D models was around 0.0049% only. The plot shows that both curves almost overlap leading us to believe that the additional simulation time utilized to step up from a 2-D model did not affect the results. The final output of the numerical modeling is reasonably close showing the superiority of the 2-D models in predicting the oil recovery from the water-wet rock for a counter-current spontaneous imbibition case within reasonable time limits.

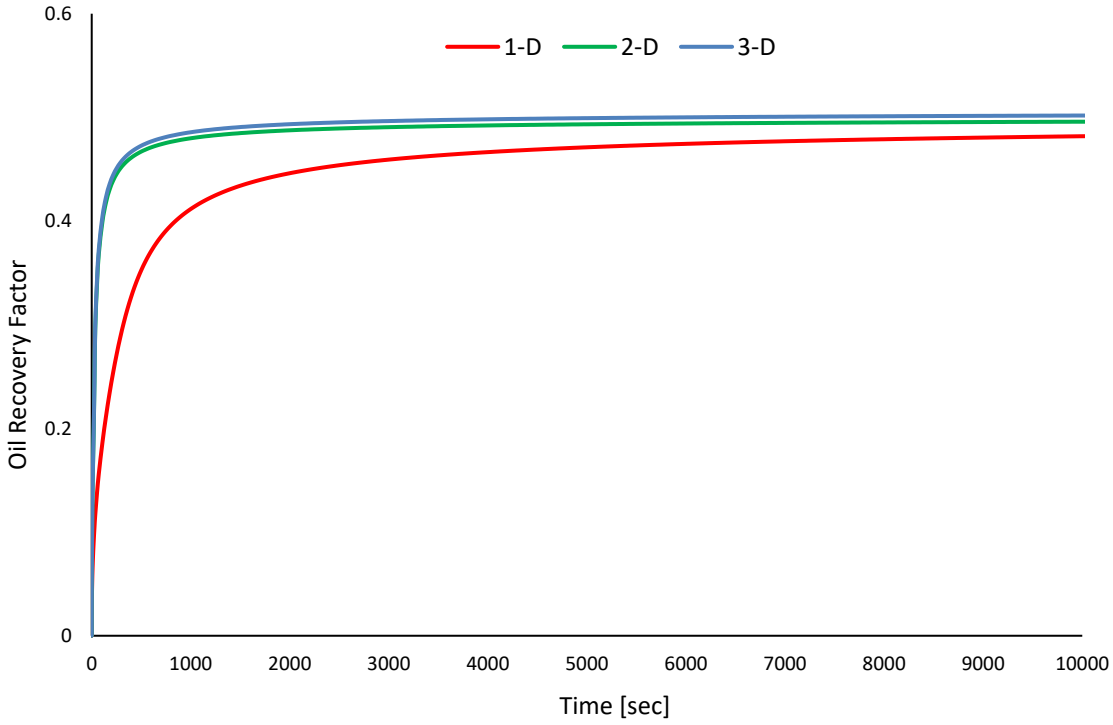

Figure 37 The plot shows recovered oil versus time for different grid sizes. There is a significant difference in the amount of oil recovered when you move from 1-D to 2-D. However, this change is minimal between 2-D and 3-D models. This could be attributed to the fact the maximum oil recovery is already reached and thus using 2-D models in satisfactory in this specific case

CHAPTER VII

SUMMARY AND CONCLUSIONS

The results of the numerical study presented in this work provide a useful insight to the Schmid and Geiger (2012) scaling group and its capability to correlate simulation results with the analytical solution in an efficient and easy manner compared to the early upscaling techniques. The following conclusions can be drawn from this work:

1) The characteristic length described by Ma et al. (1997) improved vastly the correlation between the results of the numerical model for the different boundary conditions.
2) The scaling equation developed by Schmid and Geiger (2012) used for upscaling oil recovery data significantly reduced the complexity of the mathematical operations needed to predict the oil recovery from the analytical solution. The parameters governing the spontaneous imbibition are all honored implicitly in the non-dimensional time.
3) Numerical simulations were conducted on different boundary conditions for core samples, showing that the imbibition rate is affected by the characteristic length of the geometric family of the core sample. The rate of the imbibition increases with all surface areas open to fluid exchange. The time required to achieve maximum recovery was the fastest in the AFO systems.

4) The recovery profile is AFO required refined gridding scheme to capture changes in the saturation profile at early times. The selective refinement of the grids closer to the water tanks gave more reliable recovery profile that matches with the analytical solution.
5) The number of grids used to simulate a 2-D or 3-D flow did not affect the results of the oil recovery significantly. It is advised to use a 2-D model if TEO boundary conditions for water-wet counter current spontaneous imbibition is studied. Further analysis needs to be done to make sure that this result can be generalized to the different boundary conditions used.
6) The comparison of both the analytical and the numerical models showed significant agreement between the results in general regardless of the wide range of variations within the parameters of the scaling group.
7) The initial water saturation does not have an impact on the scaling of the oil recovery. Moreover, the changes in the volume of oil displaced is analogous to the patterns predicted by experimental work.
8) The wide range of viscosity ratios did not affect the quality of the scaling of the numerical results with the analytical solution
9) The numerical results matched perfectly with the analytical solution for both counter-current and co-current spontaneous imbibition regardless of the wetness state of the rock.

REFERENCES

Akin, S., & Kovscek, A. (1999). Imbibition Studies of Low-Permeability Porous Media. *SPE Western Regional Meeting*. http://dx.doi.org/10.2118/54590-ms

Al-Lawati, S., & Saleh, S. (1996). Oil Recovery in Fractured Oil Reservoirs by Low IFT Imbibition Process. *SPE Annual Technical Conference And Exhibition*. http://dx.doi.org/10.2118/36688-ms

Andersen, P., Evje, S., & Kleppe, H. (2013). A Model for Spontaneous Imbibition as a Mechanism for Oil Recovery in Fractured Reservoirs. *Transport In Porous Media, 101*(2), 299-331. http://dx.doi.org/10.1007/s11242-013-0246-7

Alyafei, N., Al-Menhali, A., & Blunt, M. (2016). Experimental and Analytical Investigation of Spontaneous Imbibition in Water-Wet Carbonates. *Transport In Porous Media, 115*(1), 189-207. http://dx.doi.org/10.1007/s11242-016-0761-4

Amyx, J., Bass, D., & Whiting, R. (1960). *Petroleum reservoir engineering [by] James W. Amyx, Daniel M. Bass, Jr. [and] Robert L. Whiting*. New York: McGraw-Hill.

Anderson, W. (1986). Wettability Literature Survey- Part 2: Wettability Measurement. *Journal Of Petroleum Technology*, *38*(11), 1246-1262. http://dx.doi.org/10.2118/13933-pa

Arabjamaloei, R., & Shadizadeh, S. (2010). A New Approach for Specifying Imbibition Face Boundary Condition in Countercurrent Spontaneous Imbibition. *Petroleum Science And Technology*, *28*(18), 1855-1862. http://dx.doi.org/10.1080/10916460903289526

Bourbiaux, B., & Kalaydjian, F. (1990). Experimental Study of Cocurrent and Countercurrent Flows in Natural Porous Media. *SPE Reservoir Engineering*, *5*(03), 361-368. http://dx.doi.org/10.2118/18283-pa

Cil, M., Reis, J., Miller, M., & Misra, D. (1998). An Examination of Countercurrent Capillary Imbibition Recovery from Single Matrix Blocks and Recovery Predictions by Analytical Matrix/Fracture Transfer Functions. *SPE Annual Technical Conference And Exhibition*. http://dx.doi.org/10.2118/49005-ms

Clark, N. (1977). *Elements of petroleum reservoirs*. Dallas, Tex.

Cuiec, L., Bourbiaux, B., & Kalaydjian, F. (1994). Oil Recovery by Imbibition in Low-Permeability Chalk. *SPE Formation Evaluation*, *9*(03), 200-208. http://dx.doi.org/10.2118/20259-pa

Du Prey, E. (1978). Gravity and Capillarity Effects on Imbibition in Porous Media. *Society Of Petroleum Engineers Journal*, *18*(03), 195-206. http://dx.doi.org/10.2118/6192-pa

Ge, H., Yang, L., Shen, Y., Ren, K., Meng, F., Ji, W., & Wu, S. (2015). Experimental investigation of shale imbibition capacity and the factors influencing loss of hydraulic fracturing fluids. *Petroleum Science*, *12*(4), 636-650. http://dx.doi.org/10.1007/s12182-015-0049-2

Gilman, J., & Kazemi, H. (1983). Improvements in Simulation of Naturally Fractured Reservoirs. *Society Of Petroleum Engineers Journal*, *23*(04), 695-707. http://dx.doi.org/10.2118/10511-pa

Gilman, J., & Kazemi, H. (1988). Improved Calculations for Viscous and Gravity Displacement in Matrix Blocks in Dual-Porosity Simulators (includes associated papers 17851, 17921, 18017, 18018, 18939, 19038, 19361 and 20174). *Journal Of Petroleum Technology*, *40*(01), 60-70. http://dx.doi.org/10.2118/16010-pa

Hamon, G., & Vidal, J. (1986). Scaling-Up the Capillary Imbibition Process From Laboratory Experiments on Homogeneous and Heterogeneous Samples. *European Petroleum Conference*. http://dx.doi.org/10.2118/15852-ms

Huang, Y., Wang, Y., & Hou, B. (2014). Study of Spontaneous Imbibition of Water by Oil-Wet Sandstone Cores Using Different Surfactants. *Journal Of Dispersion Science And Technology*, *36*(9), 1264-1273. http://dx.doi.org/10.1080/01932691.2014.971808

Iffly, R., Rousselet, D., & Vermeulen, J. (1972). Fundamental Study of Imbibition in Fissured Oil Fields. *Fall Meeting Of The Society Of Petroleum Engineers Of AIME*. http://dx.doi.org/10.2118/4102-ms

Kazemi, H., Gilman, J., & Elsharkawy, A. (1992). Analytical and Numerical Solution of Oil Recovery From Fractured Reservoirs With Empirical Transfer Functions (includes associated papers 25528 and 25818). *SPE Reservoir Engineering*, *7*(02), 219-227. http://dx.doi.org/10.2118/19849-pa

Li, K., & Horne, R. (2004). An Analytical Scaling Method for Spontaneous Imbibition in Gas/Water/Rock Systems. *SPE Journal*, *9*(03), 322-329. http://dx.doi.org/10.2118/88996-pa

Li, K., & Horne, R. (2006). Generalized Scaling Approach for Spontaneous Imbibition: An Analytical Model. *SPE Reservoir Evaluation & Engineering*, *9*(03), 251-258. http://dx.doi.org/10.2118/77544-pa

Lucas, R. (1918). Ueber das Zeitgesetz des kapillaren Aufstiegs von Flüssigkeiten. *Kolloid-Zeitschrift*, *23*(1), 15-22. http://dx.doi.org/10.1007/bf01461107

Mason, G., Fischer, H., Morrow, N., Ruth, D., & Wo, S. (2009). Effect of sample shape on counter-current spontaneous imbibition production vs time curves. *Journal Of*

Petroleum Science And Engineering, *66*(3-4), 83-97. http://dx.doi.org/10.1016/j.petrol.2008.12.035

Mattax, C., & Kyte, J. (1962). Imbibition Oil Recovery from Fractured, Water-Drive Reservoir. *Society Of Petroleum Engineers Journal*, *2*(02), 177-184. http://dx.doi.org/10.2118/187-pa

McLean, K., Wu, S., & McAuley, K. (2012). Mean-Squared-Error Methods for Selecting Optimal Parameter Subsets for Estimation. *Industrial & Engineering Chemistry Research*, *51*(17), 6105-6115. http://dx.doi.org/10.1021/ie202352f

McWhorter, D., & Sunada, D. (1990). Exact integral solutions for two-phase flow. *Water Resources Research*, *26*(3), 399-413. http://dx.doi.org/10.1029/wr026i003p00399

Meng, Q., Liu, H., Wang, J., & Zhang, H. (2016). Effect of Wetting-Phase Viscosity on Cocurrent Spontaneous Imbibition. *Energy & Fuels*. http://dx.doi.org/10.1021/acs.energyfuels.5b02321

Morrow, N., & Mason, G. (2001). Recovery of oil by spontaneous imbibition. *Current Opinion In Colloid & Interface Science*, *6*(4), 321-337. http://dx.doi.org/10.1016/s1359-0294(01)00100-5

Muggeridge, A., Cockin, A., Webb, K., Frampton, H., Collins, I., Moulds, T., & Salino, P. (2013). Recovery rates, enhanced oil recovery and technological limits. *Philosophical Transactions Of The Royal Society A: Mathematical, Physical And Engineering Sciences*, *372*(2006), 20120320-20120320. http://dx.doi.org/10.1098/rsta.2012.0320

Muggeridge, A., Gomes, J., Mostaghimi, P., Percival, J., Tollit, B., & Pavlidis, D. et al. (2013). Reservoir Modeling for Flow Simulation Using Surfaces, Adaptive Unstructured Meshes, and Control-Volume-Finite-Element Methods. *SPE Reservoir Simulation Symposium*. http://dx.doi.org/10.2118/163633-ms

Nooruddin, H., & Blunt, M. (2016). Analytical and numerical investigations of spontaneous imbibition in porous media. *Water Resources Research*, *52*(9), 7284-7310. http://dx.doi.org/10.1002/2015wr018451

Parsons, R., & Chaney, P. (1966). Imbibition Model Studies on Water-Wet Carbonate Rocks. *Society Of Petroleum Engineers Journal*, *6*(01), 26-34. http://dx.doi.org/10.2118/1091-pa

Rangel-German, E., & Kovscek, A. (2002). Experimental and analytical study of multidimensional imbibition in fractured porous media. *Journal Of Petroleum Science And Engineering*, *36*(1-2), 45-60. http://dx.doi.org/10.1016/s0920-4105(02)00250-4

Reis, J., & Cil, M. (1993). A model for oil expulsion by counter-current water imbibition in rocks: one-dimensional geometry. *Journal Of Petroleum Science And Engineering*, *10*(2), 97-107. http://dx.doi.org/10.1016/0920-4105(93)90034-c

Relative Permeability. (2018). *Fekete.com*. Retrieved 7 February 2018, from http://www.fekete.com/SAN/WebHelp/FeketeHarmony/Harmony_WebHelp/Content/HTML_Files/Reference_Material/General_Concepts/Relative_Permeability.htm

Robin, M. (2001). Interfacial Phenomena: Reservoir Wettability in Oil Recovery. *Oil & Gas Science And Technology*, *56*(1), 55-62. http://dx.doi.org/10.2516/ogst:2001007

Saidi, A. (1983). Simulation of Naturally Fractured Reservoirs. *SPE Reservoir Simulation Symposium*. http://dx.doi.org/10.2118/12270-ms

Schmid, K., & Geiger, S. (2012). Universal scaling of spontaneous imbibition for water-wet systems. *Water Resources Research*, *48*(3). http://dx.doi.org/10.1029/2011wr011566

Schmid, K., Alyafei, N., Geiger, S., & Blunt, M. (2016). Analytical Solutions for Spontaneous Imbibition: Fractional-Flow Theory and Experimental Analysis. *SPE Journal*, *21*(06), 2308-2316. http://dx.doi.org/10.2118/184393-pa

Schmid, K., Geiger, S., & Sorbie, K. (2011). Semianalytical solutions for cocurrent and countercurrent imbibition and dispersion of solutes in immiscible two-phase flow. *Water Resources Research*, *47*(2). http://dx.doi.org/10.1029/2010wr009686

Shouxiang, M., Morrow, N., & Zhang, X. (1997). Generalized scaling of spontaneous imbibition data for strongly water-wet systems. *Journal Of Petroleum Science And Engineering*, *18*(3-4), 165-178. http://dx.doi.org/10.1016/s0920-4105(97)00020-x

Standnes, D. (2010). Scaling Group for Spontaneous Imbibition Including Gravity. *Energy & Fuels*, *24*(5), 2980-2984. http://dx.doi.org/10.1021/ef901563p

Thomas, L., Dixon, T., & Pierson, R. (1983). Fractured Reservoir Simulation. *Society Of Petroleum Engineers Journal*, *23*(01), 42-54. http://dx.doi.org/10.2118/9305-pa

Viksund, B., Morrow, N., Ma, S., Wang, W., & Graue, A. (1998). Initial water saturation and oil recovery from chalk and sandstone by spontaneous imbibition. *International Society Of Core Analysts, The Hague, September*(SCA-9814).

Warren, J., & Root, P. (1963). The Behavior of Naturally Fractured Reservoirs. *Society Of Petroleum Engineers Journal*, *3*(03), 245-255. http://dx.doi.org/10.2118/426-pa

Washburn, E. (1921). The Dynamics of Capillary Flow. *Physical Review*, *17*(3), 273-283. http://dx.doi.org/10.1103/physrev.17.273

What is Capillary Pressure Curve? - Definition from Petropedia. (2018). *Petropedia.com*. Retrieved 7 February 2018, from https://www.petropedia.com/definition/610/capillary-pressure-curve

Yildiz, H., Gokmen, M., & Cesur, Y. (2006). Effect of shape factor, characteristic length, and boundary conditions on spontaneous imbibition. *Journal Of Petroleum Science And Engineering*, *53*(3-4), 158-170. http://dx.doi.org/10.1016/j.petrol.2006.06.002

Zhang, X., Morrow, N., & Ma, S. (1996). Experimental Verification of a Modified Scaling Group for Spontaneous Imbibition. *SPE Reservoir Engineering*, *11*(04), 280-285. http://dx.doi.org/10.2118/30762-pa

Zhou, D., Jia, L., Kamath, J., & Kovscek, A. (2002). Scaling of counter-current imbibition processes in low-permeability porous media. *Journal Of Petroleum Science And Engineering*, *33*(1-3), 61-74. http://dx.doi.org/10.1016/s0920-4105(01)00176-0

APPENDIX

Sample Eclipse®-100 Coding for 2D Simulation Model of Counter-Current Spontaneous Imbibition of Water-Wet Systems with OEO

```
RUNSPEC


TITLE
2D COUNTERCURRENT HORIZONTAL - WATER-OIL SYSTEM - SWW - 2500
CELLS
-- corelength is 7.66 side is 2.5
DIMENS
-- ( number of cells present in )
-- X Y Z
51 50 1 /
-- ( phases present in system )

WATER

OIL

-- ( units )
LAB
-- ( geometry )
CART
START
-- DAY MONTH YEAR
1 JAN 2016 /
EQLDIMS
-- ( specifies dimensions of equilibration tables )
-- NTEQUL NDNPVD NDRXVD
1 100 20 /
-- default default default
TABDIMS
-- ( describes sizes of saturation & PVT tables and number of FIP regions )
-- NTSFUN NTPVT NSSFUN NPPVT NTFIP NRPVT
2 1 450 13 8 1 /
WELLDIMS
-- ( describes well dimensions )
-- MAXWELL MAXCONN MAXGROUP MAXWELLPERGROUP
1 400 1 1 /
```

UNIFOUT -- (requests for Unified output files)
GRID

----- THIS SECTION DEFINES CELL GEOMETRIES & PROPERTIES ------
---
GRIDFILE
-- (requests for GRID file export)
-- GRID EGRID
0 1 /

INIT
-- (requests for INIT file export)
-- (TRUE core measurements in cm)
DX

-- (core length)
50*0.1532 1*10
50*0.1532 1*10
50*0.1532 1*10
50*0.1532 1*10
50*0.1532 1*10
50*0.1532 1*10
50*0.1532 1*10
50*0.1532 1*10
50*0.1532 1*10
50*0.1532 1*10
50*0.1532 1*10
50*0.1532 1*10
50*0.1532 1*10
50*0.1532 1*10
50*0.1532 1*10
50*0.1532 1*10
50*0.1532 1*10
50*0.1532 1*10
50*0.1532 1*10
50*0.1532 1*10
50*0.1532 1*10
50*0.1532 1*10
50*0.1532 1*10
50*0.1532 1*10
50*0.1532 1*10
50*0.1532 1*10
50*0.1532 1*10

50*0.1532 1*10
50*0.1532 1*10
50*0.1532 1*10
50*0.1532 1*10
50*0.1532 1*10
50*0.1532 1*10
50*0.1532 1*10
50*0.1532 1*10
50*0.1532 1*10
50*0.1532 1*10
50*0.1532 1*10
50*0.1532 1*10
50*0.1532 1*10
50*0.1532 1*10
50*0.1532 1*10
50*0.1532 1*10
50*0.1532 1*10
50*0.1532 1*10
50*0.1532 1*10
50*0.1532 1*10
50*0.1532 1*10
50*0.1532 1*10
50*0.1532 1*10
50*0.1532 1*10

/

DY
-- (specifies the size of cells in the y direction)
2550*0.05 /

DZ
2550*2.5 /

-- (CORE CELLS)
BOX
-- IX1 IX2 JY1 JY2 KZ1 KZ2
1 50 1 50 1 1 /
PERMX
2500*300/
PERMY
2500*300/
PERMZ
2500*300/
PORO

```
2500*0.2 /

ENDBOX
-- ( BOTTOM CELL FULLY-SATURATED WITH WATER - 'WATER TANK' )
BOX
-- IX1 IX2 JY1 JY2 KZ1 KZ2
51 51 1 50 1 1 /
PERMX
50*10000 /
PERMY
50*10000 /
PERMZ
50*10000 /
PORO
50*1.0 /

ENDBOX
-- ( top layer specifications )
BOX
-- IX1 IX2 JY1 JY2 KZ1 KZ2
1 51 1 50 1 1 /
TOPS
2550*0 /
RPTGRID
0 0 0 0 0 1 0 0 0 1 0 0 1 /
PROPS
-------------------------------------------------------------------------------------------------
----- THIS SECTION DEFINES RESERVOIR FLUID & ROCK PROPERTIES ------
-------------------------------------------------------------------------------------------------
DENSITY
-- oil water gas (g/cm3 @ 20oC & 1atm)
0.850 1.000 0.0012 /

PVTW
-- ( PVT properties for WATER )
-- Pw(atm) Bw(rcc/scc) Cw (1/atm) Viscw(cP)
1 1 5E-05 1.0 /
PVDO
-- ( PVT properties for OIL )
-- Pg(atm) Bg(rcc/scc) Viscg(cP)
1.0 1.0001 3
1.05 1.0 3 /
ROCK
-- Pref(atm) Cr(1/atm)
```

3.0 0.5E-08 /
SWOF
-- (saturation tables for WATER & OIL)
-- (SWOF for CORE BODY)
-- Sw krw kro Pc (atm)
0.2 0 0.85 3.947692
0.201 3.125E-09 0.846814493 3.947692
0.202 2.5E-08 0.843632975 3.947692
0.203 8.4375E-08 0.840455452 3.638493739
0.204 2E-07 0.837281928 2.974846191
0.205 3.90625E-07 0.834112409 2.544646782
0.206 6.75E-07 0.830946899 2.23975562
0.207 1.07187E-06 0.827785404 2.0106565
0.208 1.6E-06 0.824627928 1.831232634
0.209 2.27812E-06 0.821474477 1.68630743
0.21 3.125E-06 0.818325057 1.566413835
0.211 4.15937E-06 0.815179671 1.465317143
0.212 5.4E-06 0.812038326 1.378731309
0.213 6.86562E-06 0.808901026 1.303605438
0.214 8.575E-06 0.805767777 1.237704259
0.215 1.05469E-05 0.802638584 1.179349776
0.216 1.28E-05 0.799513452 1.127255914
0.217 1.53531E-05 0.796392387 1.08041913
0.218 1.8225E-05 0.793275393 1.038043986
0.219 2.14344E-05 0.790162477 0.999491234
0.22 2.5E-05 0.787053643 0.964240821
0.221 2.89406E-05 0.783948897 0.931865008
0.222 3.3275E-05 0.780848245 0.902008507
0.223 3.80219E-05 0.777751691 0.874373577
0.224 4.32E-05 0.774659241 0.848708674
0.225 4.88281E-05 0.771570901 0.824799719
0.226 5.4925E-05 0.768486676 0.802463276
0.227 6.15094E-05 0.765406571 0.781541196
0.228 6.86E-05 0.762330593 0.761896342
0.229 7.62156E-05 0.759258746 0.743409166
0.23 8.4375E-05 0.756191036 0.725974944
0.231 9.30969E-05 0.753127469 0.709501511
0.232 0.0001024 0.75006805 0.69390741
0.233 0.000112303 0.747012786 0.679120362
0.234 0.000122825 0.743961681 0.665075988
0.235 0.000133984 0.740914741 0.651716744
0.236 0.0001458 0.737871972 0.638991027
0.237 0.000158291 0.73483338 0.626852415
0.238 0.000171475 0.731798971 0.615259024

0.239	0.000185372	0.72876875	0.604172961
0.24	0.0002	0.725742723	0.59355985
0.241	0.000215378	0.722720896	0.583388428
0.242	0.000231525	0.719703275	0.573630199
0.243	0.000248459	0.716689865	0.564259125
0.244	0.0002662	0.713680673	0.555251367
0.245	0.000284766	0.710675704	0.546585052
0.246	0.000304175	0.707674964	0.538240072
0.247	0.000324447	0.70467846	0.530197908
0.248	0.0003456	0.701686198	0.522441472
0.249	0.000367653	0.698698182	0.51495497
0.25	0.000390625	0.69571442	0.507723783
0.251	0.000414534	0.692734918	0.500734353
0.252	0.0004394	0.689759681	0.49397409
0.253	0.000465241	0.686788716	0.487431286
0.254	0.000492075	0.683822028	0.481095039
0.255	0.000519922	0.680859625	0.474955179
0.256	0.0005488	0.677901512	0.469002212
0.257	0.000578728	0.674947695	0.463227263
0.258	0.000609725	0.671998181	0.457622021
0.259	0.000641809	0.669052977	0.452178701
0.26	0.000675	0.666112087	0.446889998
0.261	0.000709316	0.663175519	0.441749052
0.262	0.000744775	0.660243279	0.436749411
0.263	0.000781397	0.657315374	0.431885005
0.264	0.0008192	0.654391809	0.427150116
0.265	0.000858203	0.651472592	0.422539351
0.266	0.000898425	0.648557728	0.41804762
0.267	0.000939884	0.645647225	0.413670116
0.268	0.0009826	0.642741089	0.409402294
0.269	0.001026591	0.639839326	0.405239851
0.27	0.001071875	0.636941943	0.401178714
0.271	0.001118472	0.634048947	0.397215024
0.272	0.0011664	0.631160344	0.393345117
0.273	0.001215678	0.628276141	0.389565517
0.274	0.001266325	0.625396345	0.385872924
0.275	0.001318359	0.622520962	0.382264199
0.276	0.0013718	0.61965	0.378736355
0.277	0.001426666	0.616783465	0.375286552
0.278	0.001482975	0.613921363	0.371912083
0.279	0.001540747	0.611063703	0.368610368
0.28	0.0016	0.60821049	0.365378947
0.281	0.001660753	0.605361732	0.362215472
0.282	0.001723025	0.602517435	0.359117702

0.283	0.001786834	0.599677607	0.356083496
0.284	0.0018522	0.596842255	0.353110807
0.285	0.001919141	0.594011386	0.350197678
0.286	0.001987675	0.591185006	0.347342235
0.287	0.002057822	0.588363124	0.344542685
0.288	0.0021296	0.585545745	0.341797309
0.289	0.002203028	0.582732879	0.339104463
0.29	0.002278125	0.57992453	0.336462567
0.291	0.002354909	0.577120708	0.333870106
0.292	0.0024334	0.574321419	0.331325629
0.293	0.002513616	0.571526671	0.328827739
0.294	0.002595575	0.56873647	0.326375096
0.295	0.002679297	0.565950826	0.323966412
0.296	0.0027648	0.563169744	0.321600449
0.297	0.002852103	0.560393232	0.319276016
0.298	0.002941225	0.557621298	0.316991967
0.299	0.003032184	0.55485395	0.314747199
0.3	0.003125	0.552091195	0.312540649
0.301	0.003219691	0.549333041	0.310371295
0.302	0.003316275	0.546579495	0.30823815
0.303	0.003414772	0.543830565	0.306140264
0.304	0.0035152	0.541086259	0.30407672
0.305	0.003617578	0.538346585	0.302046634
0.306	0.003721925	0.535611551	0.300049153
0.307	0.003828259	0.532881164	0.298083451
0.308	0.0039366	0.530155432	0.296148735
0.309	0.004046966	0.527434364	0.294244234
0.31	0.004159375	0.524717967	0.292369208
0.311	0.004273847	0.52200625	0.290522936
0.312	0.0043904	0.51929922	0.288704727
0.313	0.004509053	0.516596886	0.286913907
0.314	0.004629825	0.513899255	0.285149828
0.315	0.004752734	0.511206337	0.283411861
0.316	0.0048778	0.508518139	0.281699397
0.317	0.005005041	0.505834669	0.280011847
0.318	0.005134475	0.503155937	0.278348641
0.319	0.005266122	0.500481949	0.276709225
0.32	0.0054	0.497812716	0.275093062
0.321	0.005536128	0.495148244	0.273499635
0.322	0.005674525	0.492488544	0.271928438
0.323	0.005815209	0.489833623	0.270378984
0.324	0.0059582	0.48718349	0.268850798
0.325	0.006103516	0.484538153	0.267343421
0.326	0.006251175	0.481897622	0.265856406

0.327	0.006401197	0.479261905	0.264389319
0.328	0.0065536	0.47663101	0.262941739
0.329	0.006708403	0.474004948	0.261513259
0.33	0.006865625	0.471383726	0.26010348
0.331	0.007025284	0.468767354	0.258712018
0.332	0.0071874	0.46615584	0.257338496
0.333	0.007351991	0.463549195	0.25598255
0.334	0.007519075	0.460947425	0.254643826
0.335	0.007688672	0.458350542	0.253321979
0.336	0.0078608	0.455758555	0.252016673
0.337	0.008035478	0.453171471	0.250727582
0.338	0.008212725	0.450589301	0.249454389
0.339	0.008392559	0.448012055	0.248196784
0.34	0.008575	0.445439741	0.246954466
0.341	0.008760066	0.442872369	0.245727143
0.342	0.008947775	0.440309948	0.244514529
0.343	0.009138147	0.437752489	0.243316345
0.344	0.0093312	0.4352	0.242132321
0.345	0.009526953	0.432652492	0.240962194
0.346	0.009725425	0.430109974	0.239805705
0.347	0.009926634	0.427572456	0.238662605
0.348	0.0101306	0.425039948	0.237532648
0.349	0.010337341	0.42251246	0.236415596
0.35	0.010546875	0.419990002	0.235311216
0.351	0.010759222	0.417472583	0.234219283
0.352	0.0109744	0.414960215	0.233139574
0.353	0.011192428	0.412452907	0.232071874
0.354	0.011413325	0.409950669	0.231015971
0.355	0.011637109	0.407453512	0.229971661
0.356	0.0118638	0.404961446	0.228938742
0.357	0.012093416	0.402474481	0.227917018
0.358	0.012325975	0.399992628	0.226906297
0.359	0.012561497	0.397515898	0.225906394
0.36	0.0128	0.395044301	0.224917124
0.361	0.013041503	0.392577848	0.22393831
0.362	0.013286025	0.390116549	0.222969777
0.363	0.013533584	0.387660416	0.222011355
0.364	0.0137842	0.385209459	0.221062876
0.365	0.014037891	0.382763689	0.220124179
0.366	0.014294675	0.380323118	0.219195104
0.367	0.014554572	0.377887756	0.218275494
0.368	0.0148176	0.375457614	0.217365199
0.369	0.015083778	0.373032704	0.216464069
0.37	0.015353125	0.370613037	0.215571957

0.371	0.015625659	0.368198625	0.214688723
0.372	0.0159014	0.365789478	0.213814226
0.373	0.016180366	0.363385609	0.21294833
0.374	0.016462575	0.360987029	0.212090901
0.375	0.016748047	0.35859375	0.211241808
0.376	0.0170368	0.356205783	0.210400924
0.377	0.017328853	0.353823141	0.209568123
0.378	0.017624225	0.351445835	0.208743283
0.379	0.017922934	0.349073877	0.207926282
0.38	0.018225	0.346707279	0.207117005
0.381	0.018530441	0.344346054	0.206315334
0.382	0.018839275	0.341990214	0.205521158
0.383	0.019151522	0.339639771	0.204734366
0.384	0.0194672	0.337294738	0.203954849
0.385	0.019786328	0.334955126	0.2031825
0.386	0.020108925	0.332620949	0.202417217
0.387	0.020435009	0.33029222	0.201658896
0.388	0.0207646	0.327968951	0.200907438
0.389	0.021097716	0.325651154	0.200162745
0.39	0.021434375	0.323338844	0.199424719
0.391	0.021774597	0.321032032	0.198693268
0.392	0.0221184	0.318730733	0.197968298
0.393	0.022465803	0.316434959	0.197249719
0.394	0.022816825	0.314144723	0.196537442
0.395	0.023171484	0.31186004	0.195831379
0.396	0.0235298	0.309580922	0.195131445
0.397	0.023891791	0.307307384	0.194437555
0.398	0.024257475	0.305039439	0.193749628
0.399	0.024626872	0.3027771	0.193067582
0.4	0.025	0.300520382	0.192391337
0.401	0.025376878	0.298269299	0.191720817
0.402	0.025757525	0.296023865	0.191055943
0.403	0.026141959	0.293784094	0.190396642
0.404	0.0265302	0.29155	0.189742838
0.405	0.026922266	0.289321598	0.189094461
0.406	0.027318175	0.287098903	0.188451438
0.407	0.027717947	0.28488193	0.1878137
0.408	0.0281216	0.282670692	0.187181178
0.409	0.028529153	0.280465205	0.186553804
0.41	0.028940625	0.278265484	0.185931513
0.411	0.029356034	0.276071545	0.185314239
0.412	0.0297754	0.273883401	0.184701919
0.413	0.030198741	0.27170107	0.184094489
0.414	0.030626075	0.269524566	0.183491888

0.415	0.031057422	0.267353905	0.182894055
0.416	0.0314928	0.265189102	0.18230093
0.417	0.031932228	0.263030175	0.181712455
0.418	0.032375725	0.260877138	0.181128573
0.419	0.032823309	0.258730007	0.180549226
0.42	0.033275	0.2565888	0.179974358
0.421	0.033730816	0.254453533	0.179403916
0.422	0.034190775	0.252324222	0.178837845
0.423	0.034654897	0.250200883	0.178276092
0.424	0.0351232	0.248083534	0.177718606
0.425	0.035595703	0.245972192	0.177165334
0.426	0.036072425	0.243866874	0.176616227
0.427	0.036553384	0.241767597	0.176071235
0.428	0.0370386	0.239674378	0.175530309
0.429	0.037528091	0.237587236	0.174993401
0.43	0.038021875	0.235506187	0.174460465
0.431	0.038519972	0.23343125	0.173931453
0.432	0.0390224	0.231362443	0.17340632
0.433	0.039529178	0.229299784	0.17288502
0.434	0.040040325	0.227243291	0.172367511
0.435	0.040555859	0.225192984	0.171853747
0.436	0.0410758	0.22314888	0.171343687
0.437	0.041600166	0.221110998	0.170837288
0.438	0.042128975	0.219079358	0.170334508
0.439	0.042662247	0.21705398	0.169835307
0.44	0.0432	0.215034881	0.169339643
0.441	0.043742253	0.213022082	0.168847479
0.442	0.044289025	0.211015603	0.168358774
0.443	0.044840334	0.209015463	0.16787349
0.444	0.0453962	0.207021684	0.167391589
0.445	0.045956641	0.205034284	0.166913034
0.446	0.046521675	0.203053285	0.166437788
0.447	0.047091322	0.201078707	0.165965815
0.448	0.0476656	0.199110572	0.165497079
0.449	0.048244528	0.197148901	0.165031546
0.45	0.048828125	0.195193714	0.16456918
0.451	0.049416409	0.193245034	0.164109947
0.452	0.0500094	0.191302882	0.163653814
0.453	0.050607116	0.18936728	0.163200748
0.454	0.051209575	0.187438251	0.162750716
0.455	0.051816797	0.185515816	0.162303686
0.456	0.0524288	0.1836	0.161859627
0.457	0.053045603	0.181690824	0.161418506
0.458	0.053667225	0.179788312	0.160980294

0.459	0.054293684	0.177892487	0.16054496
0.46	0.054925	0.176003374	0.160112473
0.461	0.055561191	0.174120995	0.159682806
0.462	0.056202275	0.172245375	0.159255928
0.463	0.056848272	0.170376538	0.15883181
0.464	0.0574992	0.16851451	0.158410426
0.465	0.058155078	0.166659315	0.157991746
0.466	0.058815925	0.164810978	0.157575743
0.467	0.059481759	0.162969525	0.157162391
0.468	0.0601526	0.161134982	0.156751662
0.469	0.060828466	0.159307375	0.15634353
0.47	0.061509375	0.157486731	0.15593797
0.471	0.062195347	0.155673075	0.155534955
0.472	0.0628864	0.153866436	0.15513446
0.473	0.063582553	0.15206684	0.15473646
0.474	0.064283825	0.150274315	0.154340931
0.475	0.064990234	0.148488889	0.153947849
0.476	0.0657018	0.146710591	0.153557189
0.477	0.066418541	0.144939449	0.153168928
0.478	0.067140475	0.143175492	0.152783042
0.479	0.067867622	0.14141875	0.152399509
0.48	0.0686	0.139669252	0.152018306
0.481	0.069337628	0.137927029	0.15163941
0.482	0.070080525	0.13619211	0.1512628
0.483	0.070828709	0.134464528	0.150888453
0.484	0.0715822	0.132744312	0.150516348
0.485	0.072341016	0.131031496	0.150146464
0.486	0.073105175	0.12932611	0.149778779
0.487	0.073874697	0.127628188	0.149413274
0.488	0.0746496	0.125937762	0.149049927
0.489	0.075429903	0.124254866	0.148688719
0.49	0.076215625	0.122579534	0.148329629
0.491	0.077006784	0.1209118	0.147972639
0.492	0.0778034	0.119251698	0.147617727
0.493	0.078605491	0.117599264	0.147264876
0.494	0.079413075	0.115954534	0.146914066
0.495	0.080226172	0.114317544	0.146565279
0.496	0.0810448	0.112688331	0.146218496
0.497	0.081868978	0.111066932	0.145873699
0.498	0.082698725	0.109453385	0.14553087
0.499	0.083534059	0.107847728	0.145189991
0.5	0.084375	0.10625	0.144851045
0.501	0.085221566	0.104660241	0.144514014
0.502	0.086073775	0.103078491	0.144178881

0.503	0.086931647	0.101504791	0.143845629
0.504	0.0877952	0.099939182	0.143514242
0.505	0.088664453	0.098381705	0.143184703
0.506	0.089539425	0.096832405	0.142856995
0.507	0.090420134	0.095291324	0.142531103
0.508	0.0913066	0.093758506	0.142207011
0.509	0.092198841	0.092233997	0.141884703
0.51	0.093096875	0.09071784	0.141564163
0.511	0.094000722	0.089210084	0.141245376
0.512	0.0949104	0.087710775	0.140928326
0.513	0.095825928	0.08621996	0.140613
0.514	0.096747325	0.084737689	0.140299382
0.515	0.097674609	0.083264011	0.139987456
0.516	0.0986078	0.081798976	0.13967721
0.517	0.099546916	0.080342636	0.139368629
0.518	0.100491975	0.078895043	0.139061697
0.519	0.101442997	0.07745625	0.138756403
0.52	0.1024 0.076026311	0.138452731	
0.521	0.103363003	0.074605282	0.138150667
0.522	0.104332025	0.073193218	0.1378502
0.523	0.105307084	0.071790177	0.137551314
0.524	0.1062882	0.070396218	0.137253998
0.525	0.107275391	0.069011399	0.136958237
0.526	0.108268675	0.067635782	0.13666402
0.527	0.109268072	0.066269429	0.136371332
0.528	0.1102736	0.064912403	0.136080163
0.529	0.111285278	0.063564767	0.135790498
0.53	0.112303125	0.062226589	0.135502327
0.531	0.113327159	0.060897936	0.135215636
0.532	0.1143574	0.059578876	0.134930414
0.533	0.115393866	0.05826948	0.134646648
0.534	0.116436575	0.056969819	0.134364328
0.535	0.117485547	0.055679968	0.134083441
0.536	0.1185408	0.0544 0.133803975	
0.537	0.119602353	0.053129994	0.13352592
0.538	0.120670225	0.051870027	0.133249264
0.539	0.121744434	0.050620181	0.132973996
0.54	0.122825	0.049380538	0.132700106
0.541	0.123911941	0.048151182	0.132427581
0.542	0.125005275	0.046932202	0.132156411
0.543	0.126105022	0.045723685	0.131886586
0.544	0.1272112	0.044525723	0.131618095
0.545	0.128323828	0.04333841	0.131350927
0.546	0.129442925	0.042161842	0.131085073

0.547	0.130568509	0.040996119	0.130820522
0.548	0.1317006	0.039841342	0.130557264
0.549	0.132839216	0.038697615	0.130295288
0.55	0.133984375	0.037565048	0.130034586
0.551	0.135136097	0.03644375	0.129775147
0.552	0.1362944	0.035333836	0.129516961
0.553	0.137459303	0.034235425	0.129260019
0.554	0.138630825	0.033148638	0.129004312
0.555	0.139808984	0.0320736	0.12874983
0.556	0.1409938	0.031010442	0.128496563
0.557	0.142185291	0.029959297	0.128244503
0.558	0.143383475	0.028920305	0.12799364
0.559	0.144588372	0.02789361	0.127743966
0.56	0.1458	0.02687936	0.127495472
0.561	0.147018378	0.02587771	0.127248148
0.562	0.148243525	0.024888822	0.127001986
0.563	0.149475459	0.02391286	0.126756977
0.564	0.1507142	0.02295	0.126513113
0.565	0.151959766	0.022000422	0.126270385
0.566	0.153212175	0.021064314	0.126028785
0.567	0.154471447	0.020141873	0.125788305
0.568	0.1557376	0.019233304	0.125548936
0.569	0.157010653	0.018338824	0.125310671
0.57	0.158290625	0.017458657	0.1250735
0.571	0.159577534	0.016593039	0.124837417
0.572	0.1608714	0.01574222	0.124602413
0.573	0.162172241	0.014906462	0.12436848
0.574	0.163480075	0.014086041	0.124135612
0.575	0.164794922	0.01328125	0.123903799
0.576	0.1661168	0.012492398	0.123673035
0.577	0.167445728	0.011719813	0.123443312
0.578	0.168781725	0.010963847	0.123214622
0.579	0.170124809	0.010224872	0.122986959
0.58	0.171475	0.009503289	0.122760315
0.581	0.172832316	0.008799527	0.122534682
0.582	0.174196775	0.00811405	0.122310054
0.583	0.175568397	0.00744736	0.122086423
0.584	0.1769472	0.0068	0.121863782
0.585	0.178333203	0.006172567	0.121642125
0.586	0.179726425	0.005565715	0.121421445
0.587	0.181126884	0.004980168	0.121201734
0.588	0.1825346	0.00441673	0.120982987
0.589	0.183949591	0.003876305	0.120765196
0.59	0.185371875	0.00335992	0.120548354

```
0.591   0.186801472   0.00286875    0.120332456
0.592   0.1882384     0.002404163   0.120117494
0.593   0.189682678   0.001967778   0.119903463
0.594   0.191134325   0.00156155    0.119690355
0.595   0.192593359   0.001187911   0.119478165
0.596   0.1940598     0.00085       0.119266886
0.597   0.195533666   0.000552091   0.119056512
0.598   0.197014975   0.00030052    0.118847037
0.599   0.198503747   0.00010625    0.118638455
0.6     0.2     0     0.11843076
/


-- ( SWOF for 'WATER TANK' )
-- Sw krw kro Pc (atm)
0.2     0       0.85    0
0.6     1       0       0
1       1       0       0
/

RPTPROPS
2*1 0 2*1 0 2*1 /
REGIONS
------------------------------------------------------------------------
----- THIS SECTION DEFINES REGIONS OF SYSTEM ------
------------------------------------------------------------------------
SATNUM
-- ( indicates number of saturation tables )

50*1 1*2
50*1 1*2
50*1 1*2
50*1 1*2
50*1 1*2
50*1 1*2
50*1 1*2
50*1 1*2
50*1 1*2
50*1 1*2
50*1 1*2
50*1 1*2
50*1 1*2
50*1 1*2
50*1 1*2
50*1 1*2
```

50*1 1*2
50*1 1*2
50*1 1*2
50*1 1*2
50*1 1*2
50*1 1*2
50*1 1*2
50*1 1*2
50*1 1*2
50*1 1*2
50*1 1*2
50*1 1*2
50*1 1*2
50*1 1*2
50*1 1*2
50*1 1*2
50*1 1*2
50*1 1*2
50*1 1*2
50*1 1*2
50*1 1*2
50*1 1*2
50*1 1*2
50*1 1*2
50*1 1*2
50*1 1*2
50*1 1*2
50*1 1*2
50*1 1*2
50*1 1*2
50*1 1*2
50*1 1*2
50*1 1*2
50*1 1*2
50*1 1*2
50*1 1*2
50*1 1*2

/
RPTREGS
0 1 0 1 /
SOLUTION

----- THIS SECTION DEFINES INITIAL STATE OF SYSTEM -----

RPTSOL

```
'RESTART = 2' -- ( initial Restart file is created )
'FIP=1' -- ( reports initial fluids in place for whole field )
/

SWAT
50*0.2 1*1
50*0.2 1*1
50*0.2 1*1
50*0.2 1*1
50*0.2 1*1
50*0.2 1*1
50*0.2 1*1
50*0.2 1*1
50*0.2 1*1
50*0.2 1*1
50*0.2 1*1
50*0.2 1*1
50*0.2 1*1
50*0.2 1*1
50*0.2 1*1
50*0.2 1*1
50*0.2 1*1
50*0.2 1*1
50*0.2 1*1
50*0.2 1*1
50*0.2 1*1
50*0.2 1*1
50*0.2 1*1
50*0.2 1*1
50*0.2 1*1
50*0.2 1*1
50*0.2 1*1
50*0.2 1*1
50*0.2 1*1
50*0.2 1*1
50*0.2 1*1
50*0.2 1*1
50*0.2 1*1
50*0.2 1*1
50*0.2 1*1
50*0.2 1*1
50*0.2 1*1
50*0.2 1*1
50*0.2 1*1
```

50*0.2 1*1
50*0.2 1*1
50*0.2 1*1
50*0.2 1*1
50*0.2 1*1
50*0.2 1*1
50*0.2 1*1
50*0.2 1*1
50*0.2 1*1
50*0.2 1*1
50*0.2 1*1

/
PRESSURE
2550*1.0/
RPTSOL
1 0 1 1 0 0 2 7*0 0 0 0 0 /
SUMMARY

----- THIS SECTION REQUESTS FOR OUTPUT FORMATS -----

EXCEL
-- (requests output to be in MS Excel format)
RUNSUM
-- (requests a neat tabulated output of SUMMARY file data; goes into a separate RSM file)

FOIP

FWIP

BOSAT
51 1 1 /
51 2 1 /
51 3 1 /
51 4 1 /
51 5 1 /
51 6 1 /
51 7 1 /
51 8 1 /
51 9 1 /
51 10 1 /
51 11 1 /

```
51      12      1       /
51      13      1       /
51      14      1       /
51      15      1       /
51      16      1       /
51      17      1       /
51      18      1       /
51      19      1       /
51      20      1       /
51      21      1       /
51      22      1       /
51      23      1       /
51      24      1       /
51      25      1       /
51      26      1       /
51      27      1       /
51      28      1       /
51      29      1       /
51      30      1       /
51      31      1       /
51      32      1       /
51      33      1       /
51      34      1       /
51      35      1       /
51      36      1       /
51      37      1       /
51      38      1       /
51      39      1       /
51      40      1       /
51      41      1       /
51      42      1       /
51      43      1       /
51      44      1       /
51      45      1       /
51      46      1       /
51      47      1       /
51      48      1       /
51      49      1       /
51      50      1       /


/
```

```
RPTSMRY
-- ( tells ECLIPSE to print a table of variables to SUMMARY file during current run; 0 -
off; 1 - on )

1 /


SCHEDULE


----------------------------------------------------------------------------------------------------
----- THIS SECTION DEFINES TIME-DEPENDENT VARIABLES OF SYSTEM -----
----------------------------------------------------------------------------------------------------
RPTSCHED
'RESTART=2' 'SOIL' 'SWAT' 'PRES' /

MESSOPTS
ACCPTIME 2 /

WELSPECS
-- ( define well specifications )
-- NAME GROUP I J REFDEPTH(cm) PHASE
PROD G1 1 1 1 OIL /
/
COMPDAT
-- ( well completion specification data)
-- NAME I J K1 K2 OPEN/SHUT WELLBOREDIAMETER(cm)
PROD 1 1 1 1 SHUT 2* 0.0001/
/
WCONPROD
-- ( controls for PRODUCTION well )
-- NAME OPEN/SHUT
PROD SHUT BHP 5* 1.199/
/
TUNING
0.00002 0.001 0.00002 /
/
/

TSTEP
1000*0.01 /


END
```